

# **Ambient mixing ratios of ammonia during pre and post harvest paddy season in Punjab**

Saurabh Nandkumar Ramteke  
MS15063

*A dissertation submitted for the partial fulfilment of  
BS-MS dual degree in Science*



**Indian Institute of Science Education and Research Mohali  
May 2020**



# Certificate of Examination

This is to certify that the dissertation entitled “**Ambient mixing ratios of ammonia during pre and post harvest paddy season in Punjab**” submitted by **Saurabh Nandkumar Ramteke** (MS15063) for the partial fulfilment of BS-MS dual degree programme of the Institute, has been examined by the thesis committee duly appointed by the Institute. The committee finds the work done by the candidate satisfactory and recommends that the report be accepted.



Dr. A. Ambili



Dr. R. Attada



Dr. V. Sinha (Supervisor)

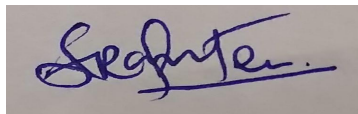
Dated: May 04, 2020



# Declaration

The work presented in this dissertation has been carried out by me under the guidance of Dr. V. Sinha at the Indian Institute of Science Education and Research Mohali.

This work has not been submitted in part or in full for a degree, a diploma, or a fellowship to any other university or institute. Whenever contributions of others are involved, every effort is made to indicate this clearly, with due acknowledgement of collaborative research and discussions. This thesis is a bonafide record of original work done by me and all sources listed within have been detailed in the bibliography.



Saurabh N Ramteke  
(Candidate)

Dated: May 04, 2020

In my capacity as the supervisor of the candidate's project work, I certify that the above statements by the candidate are true to the best of my knowledge.



Dr. V. Sinha  
(Supervisor)



# Acknowledgment

I would like to express my gratitude to Dr. Vinayak Sinha, my project supervisor for his kind supervision and guidance in completing my dissertation. I would also like to thank Dr. J. Gowrishankar, Director, IISER Mohali and Dr. Kausik Chattopadhyay, Dean R&D, IISER Mohali for providing a conducive environment which was very helpful for completing the thesis in time. I am thankful to NASA's Earth Observing System and Data Information System and Emissions Database for Global Atmospheric Research v4.2.2 for providing dataset.

I also acknowledge my lab mates for their assistance.





# List of Figures

Figure 1.1 Pie chart of the sources and sinks of ammonia

Figure 1.5.1 India's temporal ammonia distribution over the years.

Figure 1.5.2 India's sector wise source distribution and comparison for the year 2000(on the left) and 2008(on the right)

Figure 2.1.1: Location of Mohali, in the NW-IGP. Right: Map of the land use

Figure 2.2.1: Wind rose plot for the measurement site for the period of September-November 2015.

Figure 2.2.2 Diel profile of relative humidity, solar radiation and ambient temperature and for the measurement site for the period of September-November 2015

Figure 2.3.1 Schematic of the Cavity Ring down Spectroscopy

Figure 2.4.1 Ammonia original data(red) plotted with the ammonia (wind speed $<1\text{ms}^{-1}$ ) filtered data(blue) for September-November of 2015.

Figure 3.1.1 The fire counts data of VIIRS (Visible Infrared Imaging Radiometer Suite) in the months of September to November

Figure 3.1.2 (left) shows the fire count in the pre harvest season and (right)post harvest season.

Figure 3.1.3 Wind Rose plots for (left) pre harvest and (right) post harvest, September to November,2015.

Figure 3.1.4 (4m avg) Time series of the solar radiation (bottom panel), ambient temperature (middle panel) and relative humidity (top panel) denoted in yellow,red and blue respectively for September- November,2015.

Figure 3.2.1: Time series of the daily averaged mixing ratios of (in the order, from bottom to top) carbon monoxide, ammonia, acetonitrile, benzene, PM<sub>2.5</sub>, toluene and C<sub>8</sub> Aromatics (sum of xylenes and ethyl benzene) for September-November 2015.

Figure 3.3.1 Diel box and whisker profiles of a) ammonia, b) acetonitrile, c) PM<sub>2.5</sub>, d) benzene, e)toluene, f) C<sub>8</sub> aromatics(sum of xylenes and ethyl benzene), g) carbon monoxide h) ozone derived from the September- November,2015 dataset.

Figure 3.4.1.1(left) represents the correlation plot of hourly averaged ammonia and PM<sub>2.5</sub> during 09:00 to 12:00 h of the day with color scale yellow(09:00) to red(12:00), whereas(right) represents the correlation plot of hourly averaged ammonia

and PM2.5 during 16:00 to 20:00 h of the day with color scale yellow(20:00) to red(16:00), during the post harvest season.

Figure 3.4.1.2 (left) represents the correlation plot of hourly averaged ammonia and PM2.5 during 09:00 to 12:00 h of the day with color scale yellow (09:00) to red (12:00), whereas (right) represents the correlation plot of hourly averaged concentration of ammonia and PM2.5 during 16:00 to 20:00 h of the day with color scale yellow (20:00) to red (16:00), during the pre harvest season.

Figure 3.4.2.1 represents a plot between hourly averaged concentration of ammonia and ambient temperature, with  $r^2$  value of 0.90. The color scale represents the relative humidity.

Figure 3.4.3.1 plot between equilibrium constant and temperature(K) for ammonium nitrate (left) and ammonium chloride (right), increase in temperature results in a higher equilibrium constants above 302K temperature.

Figure 3.4.3.2 Hourly averaged ammonium nitrate (left) and ammonium chloride (right) concentration ( $\mu\text{g}/\text{m}^3$ ) dependence with temperature is plotted.

Figure 3.4.3.3 represents hourly averaged gas phase ammonia concentration's linear relation with temperature

Figure 3.4.3.4 represents the hourly averaged concentration of ammonium nitrate (left) and ammonium chloride (right) relation with temperature higher than 300K.



# List of Tables

Table 1.1.1 Global approximation of ammonia production from different sources.

Table 1.2.1 Summary of all ambient  $\text{NH}_3$  reactions with references and rate constants of the reactions.

Table 1.3.1 with the ambient ammonia mixing ratio reported over the world

Table 2.3.1 summarizes the the trace gas chemical specie and the characteristic wavelength used by CRDS analyser for its detection.

Table 2.3.2 summarizes the working principle of the instrument applied for measurement of said species.

Table 3.2.1 shows the gas species along with their mixing ratios in pre harvest and post harvest, the value in the bracket represents standard deviation.

Table 3.2.2 is a correlation matrix for the post harvest season of all the gas species done using daily averaged mixing ratios.





# Notation (Abbreviations)

**CCN:** cloud condensation nuclei

**NW-IGP:** North West Indo Gangetic Plain

**PM:** particulate matter

**CRDS:** Cavity Ring Down Spectroscopy

**ppb:** parts per billion

**NAAQS:** National Ambient Air Quality Standards





# Contents

<b>1. Introduction.....</b>	<b>1</b>
1.1 The global budget and the sources and sinks of ammonia.....	2
1.2 Chemical reactions of ammonia.....	4
1.3 Studies on emissions of Ammonia: Foreign and Indian Studies.....	6
1.4 Human Toxicity.....	10
1.5 Paddy residue burning in the North West-Indo Gangetic Plain (NW-IGP) and impacts on the ambient ammonia.....	12
<b>2. Material and Methods.....</b>	<b>13</b>
2.1 Site Description.....	13
2.2 General meteorology.....	15
2.3 Ambient ammonia measurement using the Wavelength Scanned- Cavity Ring Down Spectroscopy.....	17
2.4 Data quality assurance.....	19
<b>3. Results and discussion.....</b>	<b>20</b>
3.1 Demarcating pre and post harvest season and general variability in the time series of solar radiation, ambient temperature and relative humidity.....	20
3.2 General Variability in the time series of Ammonia, and the primary dataset.....	24
3.3 Diel and box whisker plot of the primary data set.....	25
3.4 Chemical Transformation of Ammonia.....	27
3.4.1 Anti Correlation with PM <sub>2.5</sub> .....	28
3.4.2 Ammonia's relation with RH and ambient temperature.....	29
3.4.3 Temperature dependence of ammonium salts.....	30
<b>4. Summary and conclusion.....</b>	<b>34</b>
<b>5. Bibliography.....</b>	<b>36</b>



# Abstract

Ammonia gas plays a key role in atmospheric chemistry as it partitions actively between gas and aerosol phase. The sources and ambient mixing ratios of ammonia are poorly known over the North West- Indo Gangetic Plain. Potentially the region is thought to be a hotspot for ammonia emissions because agriculture and biomass burning. The residue burning practice, is functional at NW- IGP after the harvesting of paddy, in October to November. This anthropogenic contamination has significant impacts on the formation of secondary inorganic aerosol particles and ill-effects on humans including irritation to the eyes, skin, nose and the respiratory system. No studies have been done yet to investigate changes in ambient ammonia mixing ratios due to paddy residue burning in the region. Other harmful gases are also emitted from the paddy residue burning such as carbon monoxide, acetonitrile, benzene and benzenoids. This study reports the measured enhancements seen in ambient ammonia in the post paddy harvest season (October 05,2015 to November 26,2015). Ammonia was quantified using the cavity ring down spectroscopy technique. Enhancements in the 4 minute averaged data were observed to be: for  $PM_{2.5}$  ( $97.2 \pm 62.1$  vs  $23.1 \pm 51.5 \mu g m^{-3}$ ), CO ( $658.9 \pm 442.7$  vs  $369.4 \pm 151.9$  ppb), acetonitrile ( $1.3 \pm 1.2$  vs  $0.5 \pm 0.3$  ppb), benzene ( $2.7 \pm 2.5$  vs  $1.4 \pm 1.1$  ppb), toluene ( $4.2 \pm 4.9$  vs  $2.1 \pm 2.2$  ppb), sum of C8 aromatics ;sum of ethyl benzene and xylenes ( $2.8 \pm 3.1$  vs  $1.7 \pm 1.3$  ppb) and ammonia ( $31.2 \pm 13.9$ .vs  $25.0 \pm 9.1$  ppb) were by a factor of 1.9, 1.8, 2.3, 1.9, 1.9, 1.6 and 1.2 respectively as compared to the pre harvest season (September 06,2015- October 04,2015). For ammonia during 09:00-12:00 hours of the day, a peak in mixing ratio is observed and it is 1.6 times than that observed in pre harvest season, clearly signifying influence of paddy residue burning emissions. The enhancement in gas phase ammonia scales with temperature and low relative humidity consistent with aerosol phase conversion of ammonium nitrate and ammonium chloride salts to gas phase ammonia. Results show active chemical processing of reactive atmospheric nitrogen which requires further investigations.

# Chapter 1

## Introduction

Ammonia ( $\text{NH}_3$ ) was first commercially produced in 1913 by combining atmospherically inert nitrogen ( $\text{N}_2$ ) and hydrogen ( $\text{H}_2$ ) to be applied as a nutrient for a crop to sustain increased population's food demand by Haber Bosch process (Hager et al. 2008, Thomas et al. 2008). Ammonia is the richest basic gas and the third most richest nitrogen containing gas (led by  $\text{N}_2$ ,  $\text{N}_2\text{O}$ ) in the atmosphere and has a pungent odor (Schlesinger et al. 1992). The fast-paced population growth has resulted in agricultural intensification and widespread enhanced fertilizer application. The nitrogen-rich fertilizer application, along with animal husbandry, is the major contributor (Clarisse et al. 2009, Fu et al. 2013) to the ambient  $\text{NH}_3$  concentrations (Aneja et al. 1998), which has risen two-folds since the pre-industrial times (Galloway et al. 2003). Industrial activities, the energy sector (coal consumption), biomass burning, such as forest fires and agricultural waste burning, also emit ammonia (Olivier et al. 1998). Ammonia shows a tendency of chemical transformation into particle-phase rather than reaction with OH radicals and also dependent on ambient temperature and relative humidity (Wang et al. 2015). Ammonium aerosols: sulfate ( $\text{SO}_4^{2-}$ ) and nitrate ( $\text{NO}_3^-$ ) are white, play a role in reflecting the solar radiation, and also act as a cloud condensation nucleus (CCN) with the implication to cloud chemistry (Charlson et al. 1990).

The ambient air quality standard for ammonia in the residential, industrial, and rural areas is  $100 \mu\text{g}/\text{m}^3$  annually and  $400 \mu\text{g}/\text{m}^3$  24 hour measurement (NAAQS,2009). The atmospheric  $\text{NH}_3$  (g) has a lifetime of 1-5 days. It is transported over to 10-100km depending upon met conditions, the ammonium particle(s) has a lifetime of 1-15 days and maybe transported long-range  $>1000\text{km}$  (Asman et al. 1998).

However, increasing anthropogenic  $\text{NH}_3$  emissions is a cause of concern. Atmospheric  $\text{NH}_3$  has adverse environmental effects as it plays a crucial role in, ecosystem eutrophication and soil acidification, and is a precursor to secondary particle formation mainly particulate matter ( $\text{PM}_{2.5}$ ) which is responsible for deteriorating air quality and smog formation (Ye et al. 2011) and various respiratory health diseases (Adams et al. 2014) and also plays a part in the neutralization of

atmospherically formed acidic gases such as sulfuric acid, hydrochloric acid and nitric acid to emit ammonium containing aerosols (Stockwell et al. 2000) which deposit onto earth surface. Therefore, it is necessary, to have a better understanding of the atmospheric chemistry and impacts of ammonia on the atmosphere and vice versa, and to carry out widespread measurements of ammonia concentration. Unfortunately, most countries in the world don't regularly monitor and/or provide incentive(s) to mitigate ammonia emissions.

## 1.1 The global budget and the sources and sinks of ammonia

Atmospheric ammonia is produced from a variety of sources, of which production and application of nitrogen-rich fertilizers, a large number of domestic animals and emissions from biomass burning are considered significant (Schlesinger et al. 1992, Hartley et al. 1992). The increased demand for meat consumption also contributes to increased animal production and hence increased ammonia emissions. According to the 2020 report on fertilizer production by the Food and Agriculture Organization of United Nations, the approximate estimate of nitrogen, potassium fertilizer is over 280 million metric tons as opposed to 1 million metric ton around 45 years ago (Aneja et al. 2001). The same report also states that average fertilizer application in 2016 was 418 kg per hectare of arable land ranging from Niger 0.4 kg/hectare (lowest) to Singapore 30297 kg/hectare (highest); in the world.

Source	Schlesinger et al. 1992 (Tg) (Tg= 10 <sup>12</sup> g)	Dentener et al. 1994 (million tons)	Bouman et al. 1997 (million tons)	EDGAR v4.2.2 2005(Gg) (Gg= 10 <sup>9</sup> g)
Agricultural	58.8	32.9	40	42271
Industrial	NA	NA	0.2	3268
Natural	14	12.1	10.8	2035
Other	2.2	NA	2.4	960
Total	75	45	53.6	48534

Table 1.1.1 Global approximation of ammonia production from different sources.

Global ammonia emissions reveal the change in emissions over the years (Schlesinger et al. 1992, Dentener et al. 1994, Bouwman et al. 1997), and database of Emissions Database for Global Atmospheric Research (EDGAR v4.2,2005) are summarized in Table 1.1.1.

From Table 1.1.1, estimations from the above studies it can be inferred that approximately 80 % of global emission of ammonia is anthropogenic and therefore there is a need for effective strategies to control and reduce such emissions.

The emissions of ammonia are classified into three major sectors: agricultural, industrial, and natural sources.

Sources: Agricultural sources include livestock farming; the production of ammonia is from the deterioration of undigested proteins, urea and uric acid by microbial and physio-chemical processes, excreta settled on the bases of accommodation fixtures, manure in a housing space and during the compost use in the fields (Oenema et al. 2006), the slurry will emit lesser ammonium particle if it is diluted with water or soil as the product will drip to the ground lower scope of vaporization of ammonia will take place (Rotz et al. 2005). The emission factors (EF) are used for different animals and are denoted in mass/year/animal and for ammonia-based EFs, they depend on temperature (Aneja et al. 2012). Agricultural sources consist of synthetic fertilizer usage and biomass burning; the use of commercialized nitrogen-containing fertilizer is the primary contributor of the production of ammonia. Urea ((NH<sub>2</sub>)<sub>2</sub>CO) is the most widely consumed fertilizer in the world at 56%, and urea contains 47% nitrogen (Behera et al. 2013). Urea is transformed to ammonium bicarbonate by urease. Ammonia emissions from fertilizer use, follow the distribution of ammonia from either the fertilizer solution in the ground or the plant to the air, the rate of production depends on the conductance or resistance to ammonia transfer (Singh and Nye et al. 1986). The production varies with a different type of fertilizer used as they vary in nitrogen content, and soil roughness property enhances ammonia production as it increases the disorders in the orifices of the soil, which grows the interaction between the ground and the air (Bajwa et al. 2008). Crop residue and bio-fuel burning may account for up-to 16% of the total emissions. The source include agriculture waste burning, forest and savanna burning and bio-fuels. Nitrogen is an essential protein that is present in all biomass and under reductive conditions, while combustion, nitrogen is reduced as ammonia (Denmead et al. 1990).

Natural sources include emissions from natural ecosystem and sea surface. A variety of microbes there in soil deteriorate organic matter and produce ammonia. Virtually all ammonia so produced is absorbed by the plant leaves in the canopy (Denmead et al. 1976) and the rate is intensified at conditions of higher relative humidity (Burkhardt

et al. 2009). The canopies also act as source and sink of ambient ammonia under low and high atmospheric ammonia concentration respectively (Langford and Fehsenfeld et al. 1992). Ambient temperature contributes in the emission and deposition of ammonia from the leaves, under stress ammonia is produced and it happens through bi-directional stomatal opening exchange. Sea surface also emit ammonia the same way, between the water surface and the air governed by the Henry's law, and through direct deposition of CCN which are made up of ammonium inorganic aerosols. Industrial sources emit ammonia in fertilizer manufacturing factories and combustion in energy sector by mainly coal.

Sinks: Ammonia is removed from the atmosphere by wet deposition(rain) on land, particle phase ammonia is removed by this process and it accounts for 30 Tg (Tg=  $10^{12}$ g)  $\text{NH}_3\text{-N/year}$ . Whereas wet deposition on sea surface accounts for 16 Tg $\text{NH}_3\text{-N/year}$ . Dry deposition of particle phase and gas phase ammonia accounts for 10 Tg $\text{NH}_3\text{-N/year}$  as differential pressure due to uneven heating causes the dry deposition. This deposition is also responsible in locating the sources.

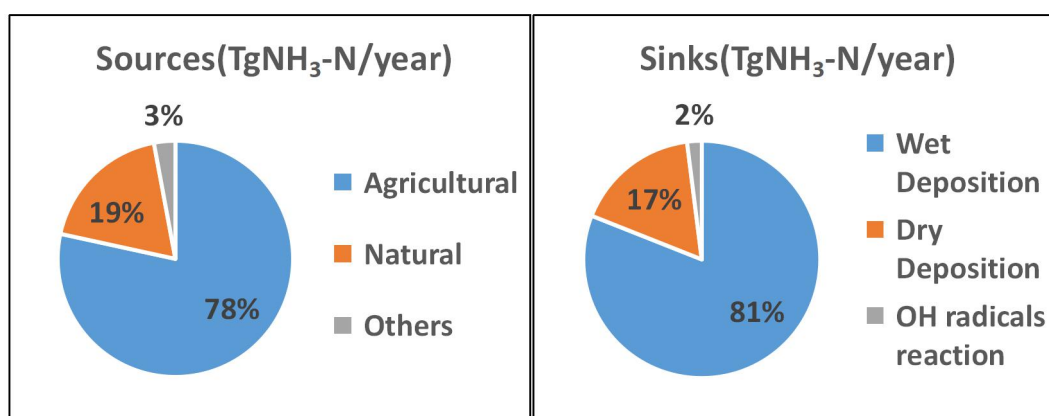


Figure 1.1 Pie chart of the sources and sinks of ammonia (Schlesinger et al 1992).

## 1.2 Chemical reactions of ammonia

### R1) Reaction of Ammonia and Sulfur Oxides:

The limiting factors for this reaction are the vapor pressure and molar ratio of the reactants. At stoichiometric 1:1 ratio;  $\text{NH}_3(\text{g}) + \text{SO}_2(\text{aq}) \leftrightarrow \text{NH}_3\text{SO}_2(\text{s})$  (yellow) and at stoichiometric 2:1 ratio;  $2\text{NH}_3(\text{g}) + \text{SO}_2(\text{aq}) \leftrightarrow (\text{NH}_3)_2\text{SO}_2(\text{s})$  (white) is produced. Both of

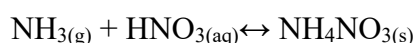
these reactions are reversible to sensitive to vapor pressure. At NTP, water in the air is at least six orders higher than that of ammonia concentration (Reverd et al. 2004) and hence SO<sub>3</sub> reacts majorly with water and not ammonia.

### R2) Reaction of Ammonia with Sulfuric acid

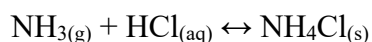
Cloud conditions act as a catalyst to convert SO<sub>2</sub> into SO<sub>4</sub><sup>2-</sup> which then reacts with moisture to form sulfuric acid. Ammonia(g) reacts with sulphuric acid in aqueous phase to form white ammonium sulphate as a component of iPM<sub>2.5</sub> (Wang et al 2006). The rate of SO<sub>2</sub> oxidation depends on the temperature and atmospheric photochemistry.  $\text{NH}_3(\text{g}) + \text{H}_2\text{SO}_4(\text{aq}) \leftrightarrow \text{NH}_4\text{HSO}_4(\text{s}) \leftrightarrow (\text{NH}_4)_2\text{SO}_4(\text{s})$ ; the ammonium sulphate product is quite stable low sensitivity to gas vapor pressure. Because of the stability of the product, new particle formation and nucleation by gas to particle transformation, it greatly influences the tropospheric PM budget.

### R3,R4) Reaction of Ammonia with Nitric acid and Hydrochloric acid:

At ambient conditions, ammonium nitrate and ammonium chloride are produced via reaction between ammonia, hydrochloric acid and nitric acid. These reactions are reversible in nature and temperature dependent.



Solid phase NO<sub>3</sub><sup>-</sup> is produced in the atmosphere by solid phase conversion beginning from the conversion of NO<sub>x</sub> to HNO<sub>3</sub>. When ambient HNO<sub>3</sub> is present, it tends to react with alkaline NH<sub>3</sub>, this reaction also is a major contributor, in urban air, of solid phase NO<sub>3</sub><sup>-</sup>.



Ammonium nitrate and ammonium chloride are, gas vapor pressure and temperature sensitive, produced under conditions suitable for gas to solid phase conversion, however unfavourable conditions favor backward reaction. Ammonia reacts the fastest with sulphuric acid followed by nitric acid and hydrochloric acid (Behera et al 2012).



### R5) Reaction of NH<sub>3</sub> with OH radical

OH radicals are able to abstract proton from ammonia to form NH<sub>2</sub> and H<sub>2</sub>O.

NH<sub>3(g)</sub> + OH ↔ NH<sub>2(g)</sub> + H<sub>2</sub>O. OH radical also acts as a sink for ammonia however the rate constant of the order 10<sup>-13</sup> makes it a lesser of an option and chemical transformation is preferred over proton abstraction.

	Reaction Information	Reference	Rate Constant (T=298 K) cm <sup>3</sup> molec <sup>-1</sup> s <sup>-1</sup>
R1	2NH <sub>3(aq)</sub> +SO <sub>2(aq)</sub> ↔ (NH <sub>3</sub> ) <sub>2</sub> SO <sub>2(s)</sub>	Landreth et al 1974	6.9×10 <sup>-11</sup>
R2	NH <sub>3(g)</sub> + H <sub>2</sub> SO <sub>4(aq)</sub> ↔NH <sub>4</sub> HSO <sub>4(s)</sub> ↔(NH <sub>4</sub> ) <sub>2</sub> SO <sub>4(s)</sub>	Finlayson et al.2006	1.5×10 <sup>-4</sup>
R3	NH <sub>3(g)</sub> + HNO <sub>3(aq)</sub> ↔ NH <sub>4</sub> NO <sub>3(s)</sub>	Pitts et al. 2006 Behera et al 2012	1.59×10 <sup>-4</sup>
R4	NH <sub>3(g)</sub> + HCl <sub>(aq)</sub> ↔ NH <sub>4</sub> Cl <sub>(s)</sub>	Zhang et al 2008 Behera et al 2012	5.16×10 <sup>-5</sup>
R5	NH <sub>3(g)</sub> + OH ↔ NH <sub>2(g)</sub> + H <sub>2</sub> O	Diau et al 1990 DeMore et al 1997	1.6 X 10 <sup>-13</sup>

Table 1.2.1 Summary of all ambient NH<sub>3</sub> reactions with references and rate constants of the reactions.

## **1.3 Studies on emissions of Ammonia: Foreign and Indian Studies**

Ammonia(g) transforms into ammonium ions(s) and is removed by deposition. Emission sources located in the proximity to lower tropospheric layer show enhanced levels of ammonia emission. It was concluded that ammonia columns' concentration from sources depended on the proximity implying only a short range transport (Erisman et al. 1987). Dry deposition expels pollutants without gas phase water vapor content as opposed to wet deposition that incorporates moisture for the liquid phase

conversion and removal from the atmosphere. Anthropogenic emissions far outweigh the natural emissions; and are dominated by industrial and agricultural emissions. According to the study of Van Damme et al. 2018, 248 ammonia hotspots were identified and isolated, and contain one or more likely sources in a limited geographical extent of less than 50km showcasing large local emission. The richest parts are the Indo-Gangetic Plain (agricultural, industrial sources), North China Plain (agricultural and industrial sources) and West Africa (biomass burning sources and agriculture). 158 hotspots belonging to industrial sources which included inadvertent losses from the production of synthetic fertiliser factories were identified and were found to be in proximity of coal related industries (coal power plants and industries using coal as fuel) compounding the ammonia production (Secunda, South Africa; Shizuishan, China). 83 hotspots belonged to agricultural sources, associated with intensive farming (Colorado, Utah in USA, Punjab, Haryana in India) and a hub of animal husbandry. 7 hotspots belonged to the natural sources that included emissions from oceans, non-agricultural soils, and other sources were too diffused to be captured by satellite, with contribution of the decay of algae in the oceans near the soda lakes (Natron, Tanzania). However, the flux calculations done with IASI (Infrared Atmospheric Sounding Interferometer) data confirmed that all the emissions from the identified hotspots were underestimated and some hotspots were slightly misplaced by one grid cell whereas some hotspots were completely absent in the emission inventory of EDGAR v4.3.1. Therefore, there is a need for a new bottom up inventory which requires new on field studies and better EFs and emission inventory.

However, satellite based studies run the risk of inaccuracies when they are not corroborated by on-field studies. Locations with prominent biomass burning practices were mostly not considered since identification of such hotspots is difficult based on emission inventory inept for dynamic fire activities emission. In high altitude areas satellite based studies for regulation and measurement of atmospheric species usually don't yield good results because of high and turbulent mixing, lesser thermal contrast and dense clouds.

	Name of the place	Latitude	Longitude	Type of Site	Measurement Time	Ambient NH <sub>3</sub> mixing ratio(ppb)	Measurement Method	Measurement Technique	Author name
1	City of Rochester	43.14618	-77.54822	Urban	April 2016 to October 2017	2.84 ± 1.91	Denuder Difference Method	nitric oxide-ozone chemiluminescence detector	2019, Chuanlong Zhou et al
2	Queens College, New York City	40.73614	73.82153	Urban	June 2016 to October 2017	3.22 ± 2.23	Denuder Difference Method	nitric oxide-ozone chemiluminescence detector	2019, Chuanlong Zhou et al
3	Pinnacle State Park	42.09142	-77.20978	Rural	April 2016 to October 2017	0.82 ± 0.64	Denuder Difference Method	nitric oxide-ozone chemiluminescence detector	2019, Chuanlong Zhou et al
4	Village of Potsdam	44.662118	-75.001016	Rural	April 2016 to October 2017	1.29 ± 1.12	Denuder Difference Method	nitric oxide-ozone chemiluminescence detector	2019, Chuanlong Zhou et al
5	Gwang Jin, Seoul	37°32'40"N	127°05'44"E	Urban	September 2010-August 2011	10.9 ± 4.25	Laser Absorption	CRDS	2013, Nhu-Thuc Phan et al
6	Gang Seo, Seoul	37°32'40"N	126°50'06"E	Urban	September 2010-August 2011	12.3 ± 4.23	Laser Absorption	CRDS	2013, Nhu-Thuc Phan et al
7	Dorset, Canada	45.224	-78.933	Rural	April 2010-April 2011	0.17	Passive Diffusive Samplers	UV-VIS Spectrometer	2012, Antoni Zbieranowski et al
8	Egbert, Canada	44.231	-79.783	Agricultural	April 2010-April 2011	1.03	Passive Diffusive Samplers	UV-VIS Spectrometer	2012, Antoni Zbieranowski et al
9	Toronto, Canada	43.709	-79.544	Urban	April 2010-April 2011	1.97	Passive Diffusive Samplers	UV-VIS Spectrometer	2012, Antoni Zbieranowski et al
10	Brussels, Canada	43.658	-81.239	Agricultural	April 2010-April 2011	3.10	Passive Diffusive Samplers	UV-VIS Spectrometer	2012, Antoni Zbieranowski et al
11	Atlanta, Georgia	33.7490° N	84.3880° W	Urban	July-December 2007	1.35 ± 1.19	Denuder Difference Method	nitric oxide-ozone chemiluminescence detector	2015, Rick D. Saylor et al
12	Yorkville, Georgia	34.0026° N	85.0416° W	Agricultural	July-December 2007	3.32±2.27	Denuder Difference Method	nitric oxide-ozone chemiluminescence detector	2015, Rick D. Saylor et al
13.	Kanpur, UP	26.449° N	80.3319° E	Urban	Summer-Winter of 2007, 2008	18.69, 19.09	Denuder Difference Method	nitric oxide-ozone chemiluminescence detector	2010, Sailesh N. Behera et al
14	Waliguan, China	36°17'N	100°55'E	HA	January 2007-December 2008	4.0± 2.9	Passive Samplers	Ion chromatography	1982, Zhao-Yan Meng
15	Mt. Sonnblick, Switzerland	12°57'E	47°03'N	HA	November 1991-November 1993	15±14( Summers) 3.3±3.6(winters)	Passive Samplers	Ion chromatography	1982, ANNE KASPER et al

TABLE 1.3.1 with the ambient ammonia mixing ratio reported over the world

Table 1.3.1 compiles the data from on-field studies done at rural, agricultural, urban and high altitude (HA) areas with reported ammonia mixing ratios and measurement techniques which provide the required contrast with respect to satellite based studies. The highest reported mixing ratio is for (urban setting) Kanpur, India at 17 ppb (24h measurement) and lowest reported mixing ratio is for (rural setting) Dorset, Canada at 0.17 ppb (24h measurement). Usually the urban setting's emissions are coupled with agricultural and industrial sources and transport sector (vehicular emission). The high altitude areas showed a maxima in summer at 15 ppb for Mt Sonnblick, Switzerland with high uncertainty (14 ppb). Highest agricultural emission is from Yorkville, Georgia at 3.32 ppb. The methods used for the measurements of the studies done are CRDS, UV-Vis Spectrometer, NO-O<sub>3</sub> chemiluminescence detector and ion chromatography. CRDS uses laser absorption and more details are provided in Chapter 2. Ion chromatography has the advantage of measuring both gas phase as well as solid phase ammonium particles, inorganic water soluble PM<sub>2.5</sub> are dissolved in water and quantified through the difference in their ion mobility. The gas phase ammonia is measured directly through NO-O<sub>3</sub> chemiluminescence detector where ammonia is oxidized and measured NO through one valve where as the other valve measures NO, the difference between the two valves gives the mixing ratio of ammonia. UV-Vis Spectrometer requires the offline samples taken to be prepared before analysing, for ammonia it absorbs at 210 nm and a xenon arc lamp is used for the excitation of the ammonia molecules, the absorption follows the Beer-Lambert's law. In India for the summer and winter of 2007-08 ambient ammonia mixing ratios were reported by Behera et al 2010 and they were found out to be 18.69 ppb and 19.09 ppb respectively. The ammonium ions in summer gets chemically transformed into ammonia gas; lesser amounts of ammonium aerosol were also observed, and in winter season the region of Kanpur experiences the events of biomass burning; enhancing the ammonia mixing ratio.

Seoul and Kanpur, urban but connected to rural agricultural sites showed much significantly higher ambient values with 10.9 ppb and 12.3 ppb for two sites in Seoul and 17.1 ppb for Kanpur.

Along the fairly similar latitudes, in the City of Rochester and Village of Potsdam in the New York city, the mixing ratios (2.84 ppb and 1.29 ppb resp.) found were marginally different than one another owing to the differences in source's emissions. City of Rochester and Queens College, New York and; Village of Potsdam and

Pinnacle State Park showed fairly similar mixing ratios (2.84ppb and 3.2ppb resp.; and 1.29ppb and 0.82ppb) due to the similarity in their emissions from fairly similar sources. At Atlanta (urban) and Yorkville (agricultural), the mixing ratios found to be were 1.35ppb and 3.32ppb, stark difference was observed owing to the less industrialized urban area emitting less ammonia than the rural agricultural area with emissions from poultry farms and use of synthetic fertilizers.

## **1.4 Human Toxicity**

Ammonia is component in atmosphere, lithosphere and hydrosphere and is emitted by anthropogenic and natural causes and is found in manures, fertilizers and different cleaning products. One is exposed to excessive ammonia by direct breathing in ammonia from sources. Excessive amounts of ammonia affects the respiratory tract during inhalation and damages the respiratory system and burning sensations at the site of contact such as eyes, nose and mouth. Long term exposure to ambient ammonia may enhance the risk of respiratory irritation, cough, wheezing, tightness in the chest, and impaired lung function in humans (EPA,2016,Toxicological report of ammonia).

## **1.5 Paddy residue burning in the North West-Indo Gangetic Plain (NW-IGP) and impacts on the ambient ammonia.**

Over the years in India, the anthropogenic emissions have risen mainly due to the agriculture sector's contribution by the application of nitrogen rich fertilizers, livestock manure management. Energy (combustion and non combustion) Sector has also been significantly rising to meet the urbanisation energy demand and hence these sources also contribute to the emissions of ammonia. The trend is of upwards trajectory and necessary steps need to be taken so as to prevent the ecosystem from further damage. India's ammonia emission in 2008 was 4241 Gg NH<sub>3</sub>-N per year (Gg=10<sup>9</sup> g) has risen roughly four-folds since 1970 when it was 1107 Gg NH<sub>3</sub>-N per year.

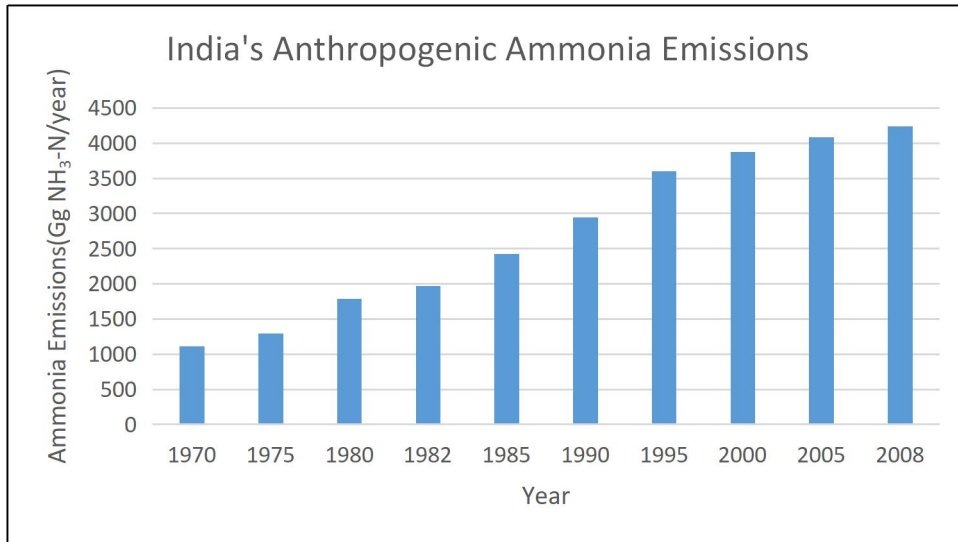


Figure 1.5.1 India's temporal ammonia distribution over the years.(EDGAR v4.2.2)

From 2000 to 2008, the energy sector as well as agriculture sector has seen an upward trend in emission. This is due to adapting to modern industrialization and greater use of ammonium based fertilizers, rise in the population of domestic animals and agriculture burning. However, forest and grassland fires have become less frequent with lower emissions when comparing the two years (2000,2008). In 2008, energy sector (coal combustion and non combustion based sources) contributed to 98 Gg NH<sub>3</sub>-N per year, compared to 91 Gg NH<sub>3</sub>-N per year in the year 2000. The agricultural sector(direct soil emissions, fertilizer usage and agricultural waste burning) emissions of ammonia have grown significantly by 372 Gg NH<sub>3</sub>-N from 2008 (4263 Gg NH<sub>3</sub>-N/year) to 2000 (3891 Gg NH<sub>3</sub>-N/year).

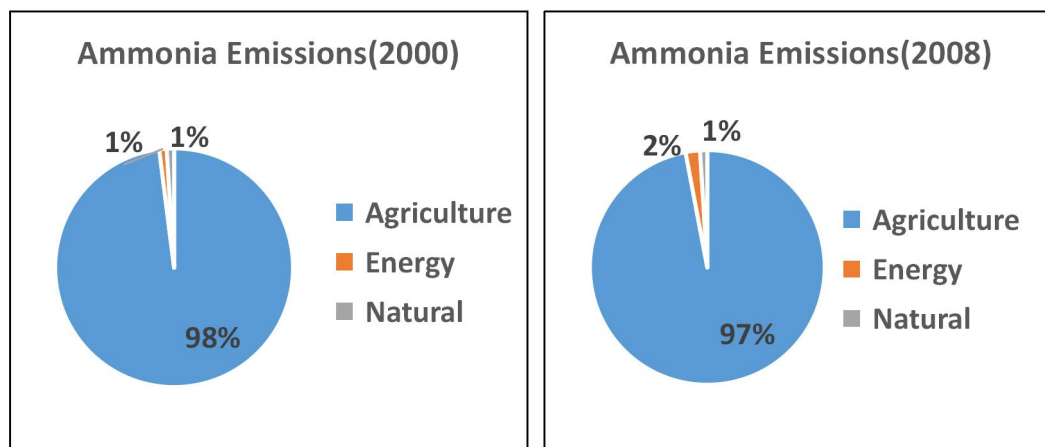


Figure 1.5.2 India's sector wise source distribution and comparison for the year 2000(on the left) and 2008(on the right) (source EDGAR v4.2.2)

In 2008, the breakdown of agricultural sources suggests direct soil emissions are 76% of all production (3312 Gg NH<sub>3</sub>-N/year) and manure management is 19% of all production (826 Gg NH<sub>3</sub>-N/year) and the agricultural waste burning is 3% of all production (130 Gg NH<sub>3</sub>-N/year) while the other minor sources rounded off the total emissions.

In the Indian state of Punjab, the sowing of paddy generally starts at the end of month may and lasts till end of July. Extensive post crop harvest fires occur during October-November. This anthropogenic perturbation is the reason for contamination of post monsoon air, and demarcating post polluted monsoon season, with harmful effects on regional air quality with carcinogens such as benzene, and benzenoids and carbon monoxide is also produced from these fire events. This practice became famous after the beginning of the combine harvester technology that removed the grains from the paddy crops but left the crops (stubble) standing in the field . The most convenient removal practise is to burn the standing paddy residue which enhances multitude of harmful gases and particle phase particles. To visualize the degree of the area spread of the paddy residue burning, Punjab in India (80% of the land associated for agriculture), accounted for 12,685 km<sup>2</sup> in 2005 (Badrinath et al.2006) whereas crop residue burning for entire India accounts for 289 Tg (Venkatraman et al 2006) (More information about the impact of paddy residue burning for the year 2012-14 of benzene and benzenoids is provided in Chandra et al. 2016).

Acetonitrile (biomass burning chemical marker) enhancement is the characteristic of the post monsoon pollution. Ammonia concentrations also see enhancement in this season, while major sources of ammonia are direct soil emissions due to fertilizer application, the agricultural waste burning does play a role in the increased ambient concentration of ammonia. In 2008, direct soil emissions accounted for 76 percent of the total emissions whereas the agricultural waste burning accounted for a mere 3 percent. But this satellite derived data has not been corroborated with on field studies. The highest in the world was reported at the Indus Valley (Pakistan) at  $1.1 \times 10^{17}$  molecules/cm<sup>2</sup>.

My thesis proposes to investigate the sources and sinks, mechanisms via which chemical transformation of ammonia in the pre and post harvest due to paddy residue burning by using Wavelength Scanned-Cavity Ring Down Spectroscopy (WS-CRDS) online measurement method.

# Chapter 2

## Material and Methods

### 2.1 Site Description

All of the observations, in this thesis, were carried out at the Central Analytical Facility(CAF) of the Indian Institute of Science Education and Research (a sub-urban site in the city Mohali). Figure 2.1.1(left) shows the position of the measurement site in Mohali, super-imposed on a land-use map in the NW-IGP proximate to the foothills of the Himalayan mountain range. Figure 2.1.1 (right) shows the precise location of neighboring cities and the Himalayan mountain range. The campus is residential surrounded by a National Highway and a few industries.

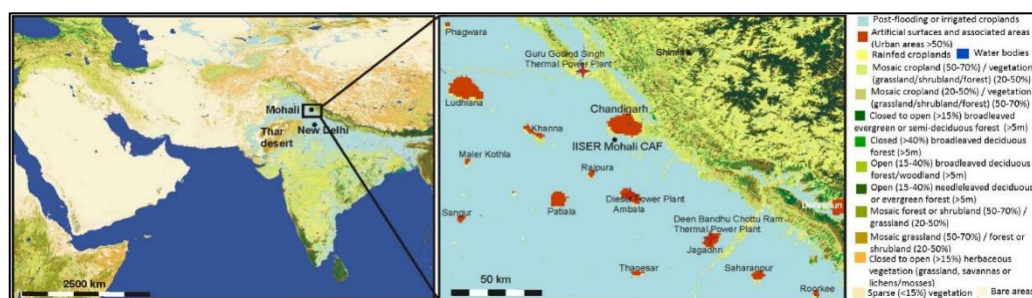


Figure 2.1.1: Left: Location of Mohali, in the NW-IGP. Right: Map of the land use in a 100 km × 200 km area surrounding the measurement site (black dot, 30.667° N, 76.729°E, 310 m asl)

The east region wind sector covering 0<sup>0</sup>-90<sup>0</sup> consists of the urban setting of Chandigarh and Panchkula in the proximity of the measurement facility. This region and emissions from it are differentiated as urban sources. The wind sector covering 90<sup>0</sup>-180<sup>0</sup> from east-south has the presence of industrial as well as agricultural field land. This sector has industries of solvent, paint, pharmaceutical and glass manufacturing and a National Highways 1 and 2. The wind sector covering 180<sup>0</sup>-360<sup>0</sup> South to North is predominantly agricultural-based land use.



## 2.2 General meteorology

Wind speed, wind direction, ambient temperature and solar radiation were measured at the institute applying meteorological sensors (Met One Instruments Inc., Rowlett, Texas, USA) at a temporal resolution of 1 minute. Figure 2.2.1 represents the wind rose plots for the period of study: September 6, 2015, to November 25, 2015. Figure 2.2.2 shows the diel profile of the solar radiation, ambient temperature and relative humidity for the period of study along with their associated variability.

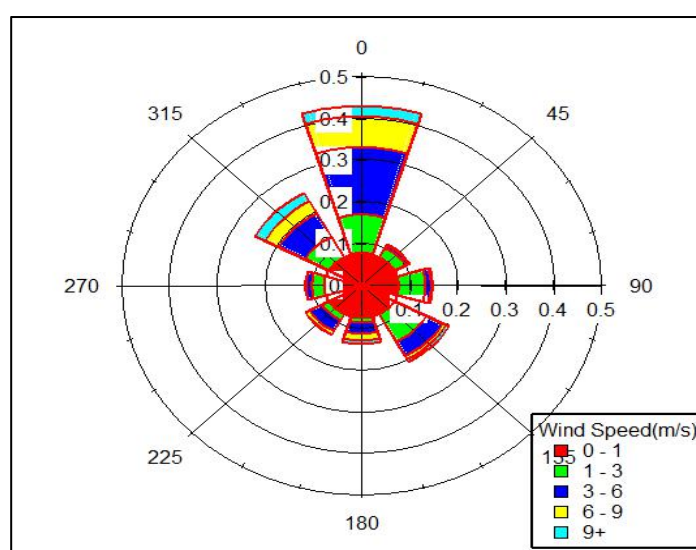


Figure 2.2.1: Wind rose plot for the site of the study (30.667N, 76.729 E, 310 ma.s.l.) for the period of September-November 2015.

The months of September-November are associated with monsoon and post-monsoon seasons and warm days in which day time average solar radiation peaked at  $\sim 600 \text{ Wm}^{-2}$  between 11:00 and 12:00. The average ambient temperature remained above  $22^{\circ}\text{C}$  and reached as high as  $30^{\circ}\text{C}$  between 12:00 and 15:00. The average maximum and minimum relative humidity ranged between 48% at 14:00 and 80% at 00:00

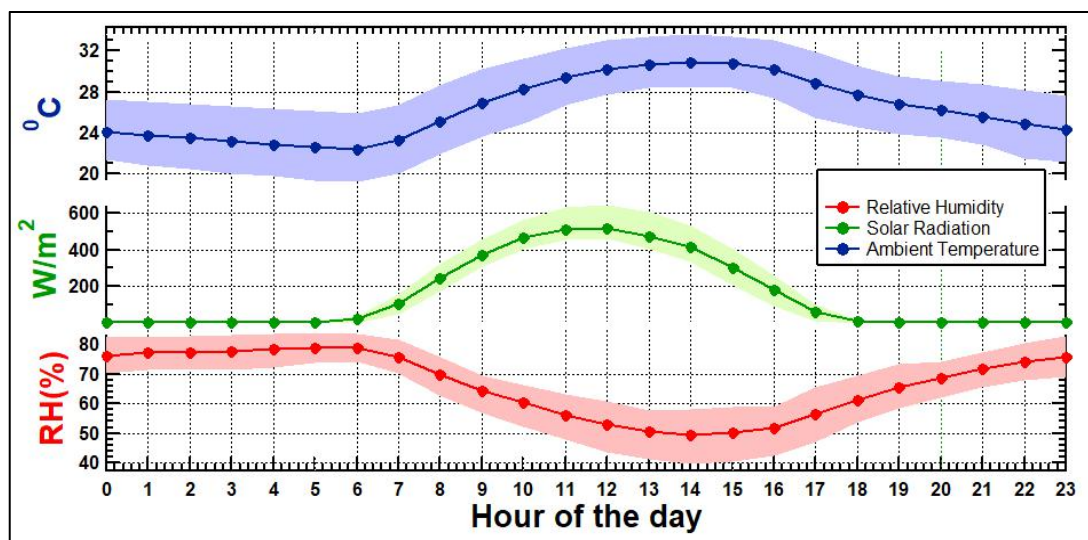


Figure 2.2.2 Diel profile of relative humidity, solar radiation and ambient temperature and for the measurement site for the period of September-November 2015 (in that order from bottom to top). Markers represent hourly average and the shaded region on the top and bottom represents the 75<sup>th</sup> and 25<sup>th</sup> percentile.

The duration of September-November was selected due to the functionality of large scale biomass burning that occurs in the NW-IGP region which contaminates the air quality level in the post (polluted) monsoon season.

Wind speed  $< 1 \text{ ms}^{-1}$  accounted for 7.8 % of the total duration and was removed to analyze regionally representative mixing ratios of ammonia influenced by paddy residue burning. Predominant wind direction is north to northwestern spanning the time of the study. This wind direction occurred for ~42 % of the time-spanning duration of the study. This fetch region was also associated with high wind speeds which means long-range transport of ammonia towards the measurement facility. Wind speeds for this region with predominant wind direction varied from 1 to 10 m/s for ~95% of the time. Higher wind speeds were generally observed during rain events.

## 2.3 Ambient ammonia measurement using the Wavelength Scanned- Cavity Ring Down Spectroscopy

Cavity Ring Down Spectroscopy (CRDS) is a high precision, low drift technique that uses an optical cavity and laser (absorption at a characteristic wavelength, table 2.3.1 for details) set up, for the simultaneous measurement of 5 infrared active trace gases, in the parts per billion range. The CRDS analyser (Model G2508, Picarro, Santa Clara, USA) was used in this study for the online measurement of ammonia, at a 4m temporal resolution. A gas sample is injected into the high finessed optical cavity where, the sample is subjected to tunable semiconductor diode laser beams and the absorbance determination, hence providing the concentration of the required chemical specie. The instrument is made up of the laser, optical cavity, three mirrors and a photo-detector. The light from the laser is introduced into the cavity through the convergent lens to a partially reflective mirror (reflectivity >99.99%). Light in the cavity travels 100,000 times for an estimated approximation of 20km (Instrument manual, Picarro), and remains in the cavity for a long time enabling the measurements with high precision. The light intensity developed over time and is monitored by a photodetector through a second partially reflective mirror. The third mirror is placed in the optical cavity such that all of the mirrors form an isosceles triangle (figure 2.3.1 for schematic diagram). The ring down measurement is done by frequently switching off the laser and measuring the light intensity decaying exponentially with respect to a time constant,  $\tau$ .

<b>Gas Specie</b>	<b>Patented Wavelength</b>
CO <sub>2</sub>	1.603 $\mu\text{m}$
CH <sub>4</sub>	1.659 $\mu\text{m}$
H <sub>2</sub> O	1.561 $\mu\text{m}$
NH <sub>3</sub>	1.527 $\mu\text{m}$
N <sub>2</sub> O	4.460 $\mu\text{m}$

Table 2.3.1 summarizes the the trace gas chemical specie and the characteristic wavelength used by CRDS analyser for its detection. (Crosson et al. 2008)

There are two loss mechanisms at play here, one due to the imperfect reflectivity of the mirrors and second due to the absorption and scattering of the gas sample. The analyzer repeatedly scans the laser over individual gas specie spectral features and notes the loss at characteristic wavelength. The individual absorption spectrum of the gases is a function of optical frequency. The temperature and pressure of the cavity is maintained at 45<sup>0</sup>C and 140 Torr which result in highly stable spectroscopic features.

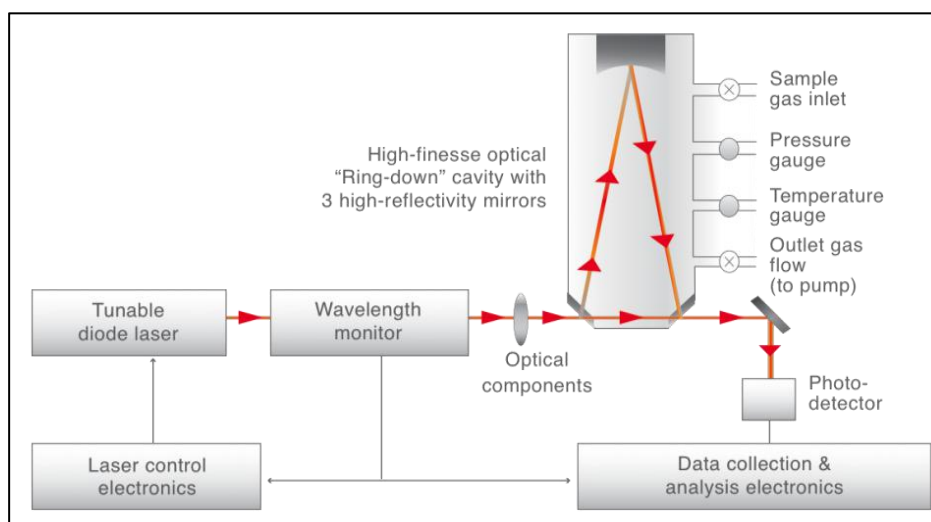


Figure 2.3.1 Schematic of the Cavity Ring down Spectroscopy (Picarro instrument manual)

The primary data set also contains data of CO, several VOCs and PM2.5 along with ammonia and instrument and working principle is provided in Table 2.3.2.

Instrument	Working Principle	Species
CO analyser	Non Dispersive Infrared Spectroscopy	CO
PM2.5 Analyser	Beta Attenuation	PM2.5
PTRMS	Chemical Ionization Mass Spectroscopy	VOCs
CRDS	Laser Absorption Spectroscopy	Ammonia

Table 2.3.2 summarizes the working principle of the instrument applied for measurement of said species.

## 2.4 Data quality assurance

The study focuses on the regional signatures pertaining to ammonia emissions due to the biomass burning activities and therefore in order to remove extremely local influences a wind speed filter ( $<1\text{ms}^{-1}$ , 7.8% of the dataset removed) was used. Figure 2.4.1 graphically represents data optimization with the wind speed filter.

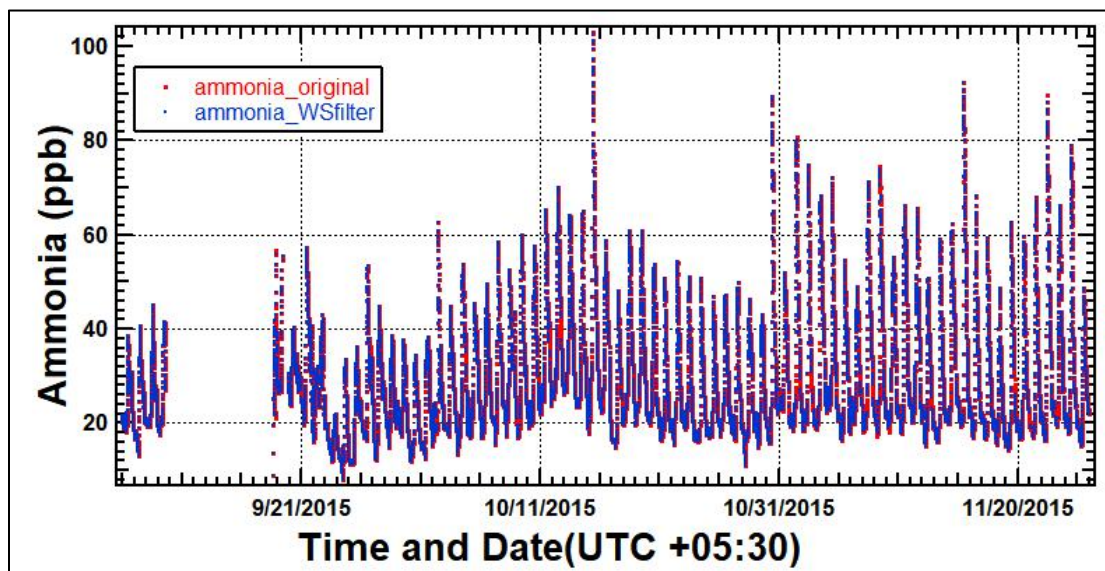


Figure 2.4.1 Ammonia original data(red) plotted with the ammonia (wind speed  $<1\text{ms}^{-1}$ ) filtered data(blue) for September-November of 2015.

# Chapter 3

## Results and discussion

### 3.1 Demarcating pre and post harvest season and general variability in the time series of solar radiation, ambient temperature and relative humidity

The period of September to November is divided into two hypothetical (pre and post harvest) seasons for the ease of understanding and to study the effects of paddy residue burning enhancement seen in ammonia and various other gases. The data from VIIRS (Visible Infrared Imaging Radiometer Suite) onboard National Oceanic and Atmospheric Administration-20 satellite was used to demarcate the post harvest season from the pre harvest season over the region in the black box(Figure 3.1.2) for September to November, 2015. The spatial resolution of this sensor is 500m x 500m (better than 1km x 1km of MODIS Aqua and Terra) and the bypass over the region denoted in the block box(Figure 3.1.2) is twice(07AM and 07PM, UTC converted). The VIIRS data is categorized in three sections: lower, moderate and higher with respect to confidence interval of the data.

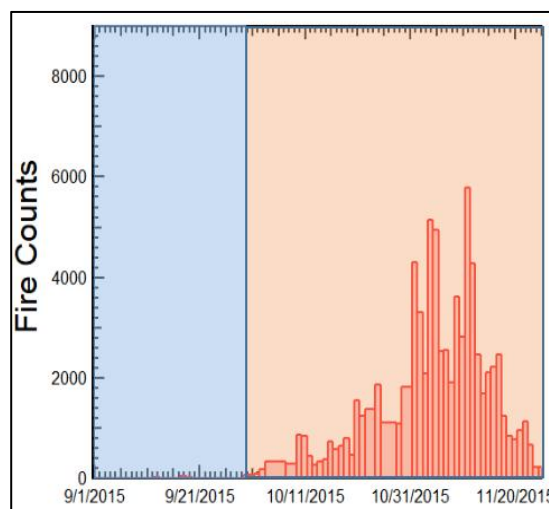


Figure 3.1.1 The fire counts data of VIIRS (Visible Infrared Imaging Radiometer Suite) in the months of September to November over the region enclosed in the black

box (refer to Figure 3.1.2), the data belonging to moderate and high confidence interval was used.

The fire counts on October 5, 2015 were 376 and the highest number of fire counts(5826) were recorded on November 10,2015. The fire counts in September 1,2015-October 4,2015 were 1529 and October 5,2015- November 25,2015 were 79,804 and the average number of fires detected for the same time frame is 58 and 1734 respectively. To minimize false fire positives, only fire counts belonging to moderate and high confidence interval were analyzed. The fire counts with lower confidence interval were eliminated. Hence, adding a basis for differentiating the seasons as pre harvest(September 06,2015 to October 04, 2015) and post harvest(October 4,2015 to November 25, 2015).

The bifurcation of pre and post harvest season dates in 2015 were done by following basis: VIIRS fire count activity data(figure 3.1.2) and the consistency of the fetch region and meteorologic conditions(figure 3.1.3). The comparability in meteorology and fetch region makes sense for analyzing the crop residue burning events on atmospheric chemical concentration enhancement.

Figure 3.1.2 represents VIIRS fire count data for the months of September to November for the black box region enclosing the major agricultural regions in NW-IGP between 28<sup>0</sup>N to 33<sup>0</sup>N and 72<sup>0</sup>E to 79 <sup>0</sup>E, the measurement site is located at 30.667°N, 76.729°E.

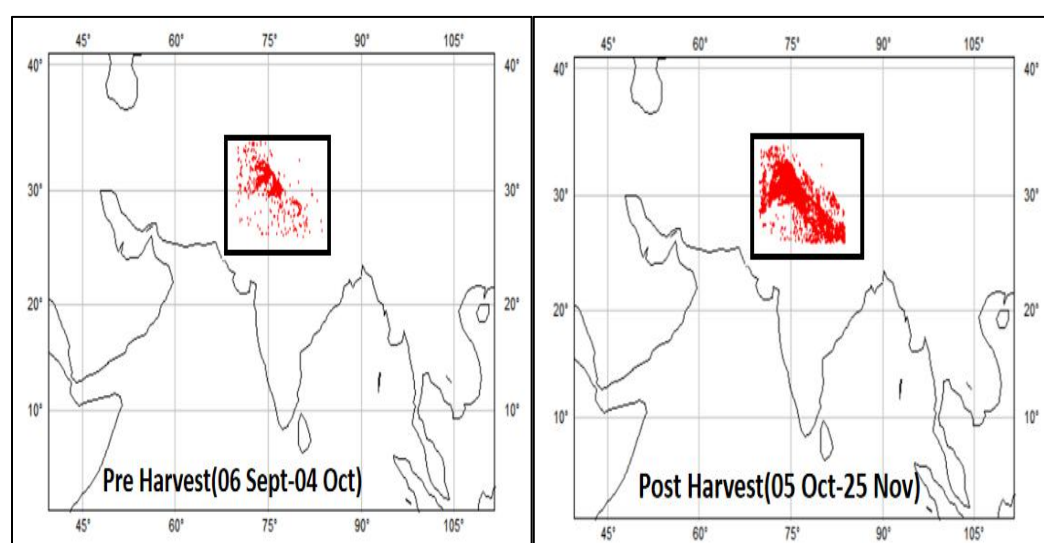


Figure 3.1.2 (left) shows the fire count in the pre harvest season and (right) post harvest season. The black square boxes cover the Punjab, and portions of Himachal Pradesh, Haryana and Uttar Pradesh.

Figure 3.1.3 shows the fetch region and the corresponding wind direction and wind speed. This is specially important while assessing the post harvest burning impact on the mixing ratios of the concerned chemical species.

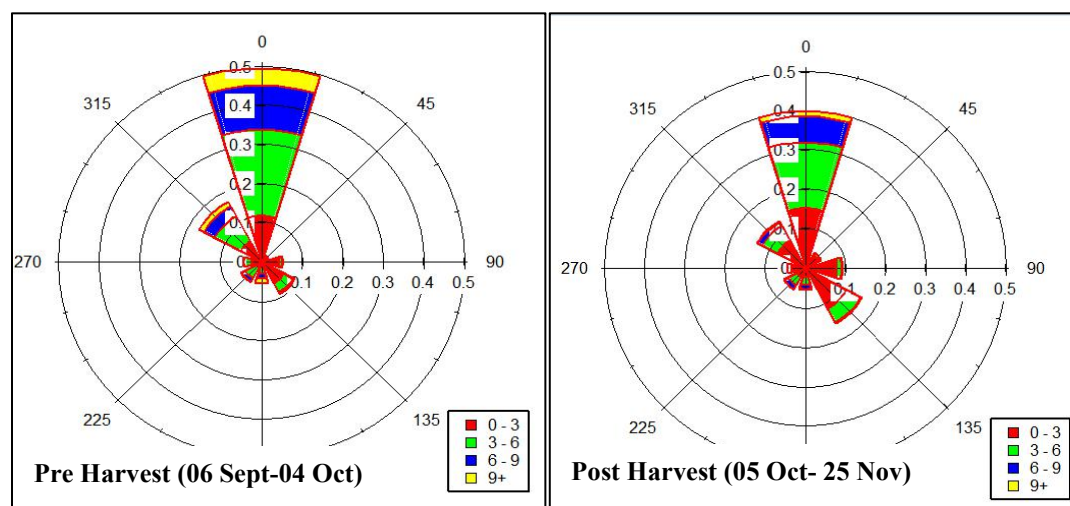


Figure 3.1.3 Wind Rose plots for (left) pre harvest and (right) post harvest, September to November, 2015.

The median wind direction in both, pre and post harvest is from north and northwest side, where the agricultural fields are located. Most of the ammonia emissions is from the agricultural sector. The average wind speeds were comparable for the two seasons; pre harvest season with  $4.5 \pm 2.8 \text{ ms}^{-1}$  and post harvest season it with  $3.3 \pm 2.3 \text{ ms}^{-1}$ . The average ambient temperature for the pre harvest season was  $27.9 \pm 3.4 \text{ }^{\circ}\text{C}$  and;  $23.2 \pm 4.5 \text{ }^{\circ}\text{C}$  for the post harvest season, the average temperature. The average relative humidity for the pre harvest season was  $71.1 \pm 13.6 \%$  and  $60.3 \pm 14.9 \%$  for the post harvest season. The decline in average temperature, of about 16%, and average relative humidity, of about 15%, is observed and as the transition from pre harvest to post harvest season takes place. Ambient temperature along with relative humidity play a vital role in the partition functionality of ammonia. The before-after mixing ratios of acetonitrile and other biomass burning related emissions also validate this bifurcation of seasons and is discussed in detail in 3.2 section. Hence, the demarcation of the seasons as; pre harvest (September 06, 2015 to October 04, 2015) and post harvest (October 4, 2015 to November 25, 2015) is followed.



Figure 3.1.4 shows the 4m temporal distribution of solar radiation, ambient temperature and relative humidity; from September 6,2015 to November 25,2015.

The lowest average ambient temperature ( $18\text{ }^{\circ}\text{C}$ ) was observed at 06:00 hour of the day and the highest average ambient temperature ( $32\text{ }^{\circ}\text{C}$ ) was observed at 14:00 hour of the day. The average ambient temperature, during September to November 2015, was  $24.8\pm 4.7\text{ }^{\circ}\text{C}$ .

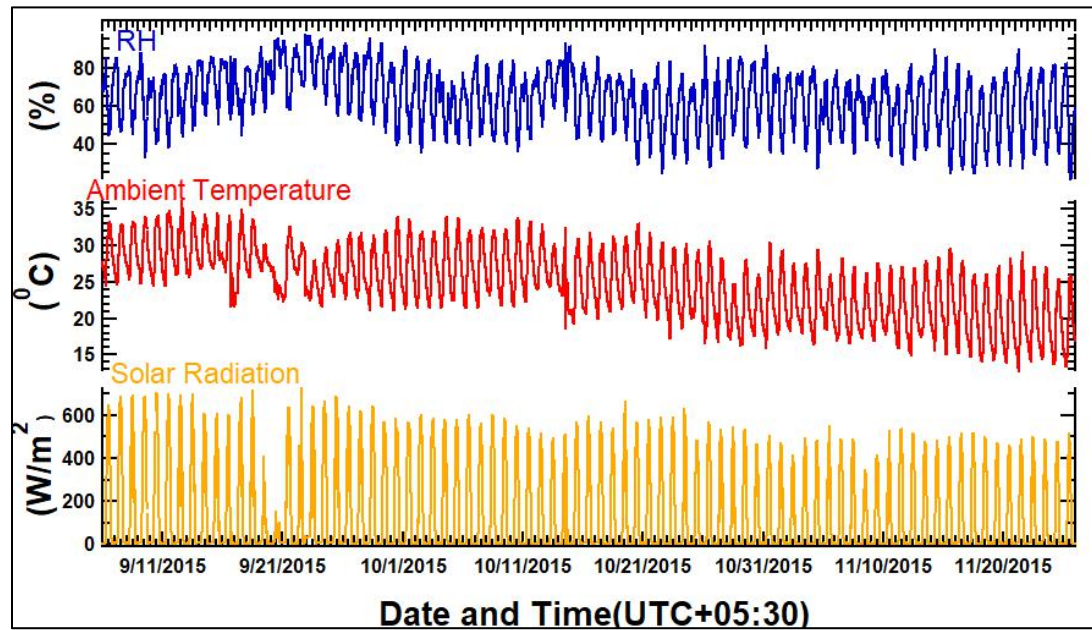


Figure 3.1.4 (4m avg) Time series of the solar radiation (bottom panel), ambient temperature (middle panel) and relative humidity (top panel) denoted in yellow,red and blue respectively for September- November,2015.

The average solar radiation is non zero starting from 06:00 to 18:00 hour of the day and the highest value ( $541\text{ W/m}^2$ ) was observed at 12:00, and remains zero for the rest of the hours. The average solar radiation, during September to November 2015, was  $150\text{ W/m}^2$ .

The lowest average relative humidity (38%) was observed at 14:00 hour of the day and the highest average relative humidity (82%) was observed at 06:00 hour of the day. The average relative humidity, during September to November 2015, was  $64.2\pm 15.4\%$ .

Ambient temperature and solar radiation are correlated with each other while both anti-correlates with relative humidity.

### 3.2 General Variability in the time series of Ammonia, and the primary dataset

Figure 3.2.1 shows the time series of daily averaged ambient mixing ratios of carbon monoxide, ammonia, acetonitrile, benzene, PM2.5, toluene and sum of C8 aromatics isomers for September-November 2015. The shaded region in each plot corresponds to the 25<sup>th</sup> and 75<sup>th</sup> percentile respectively, indicating the daily ambient variability.

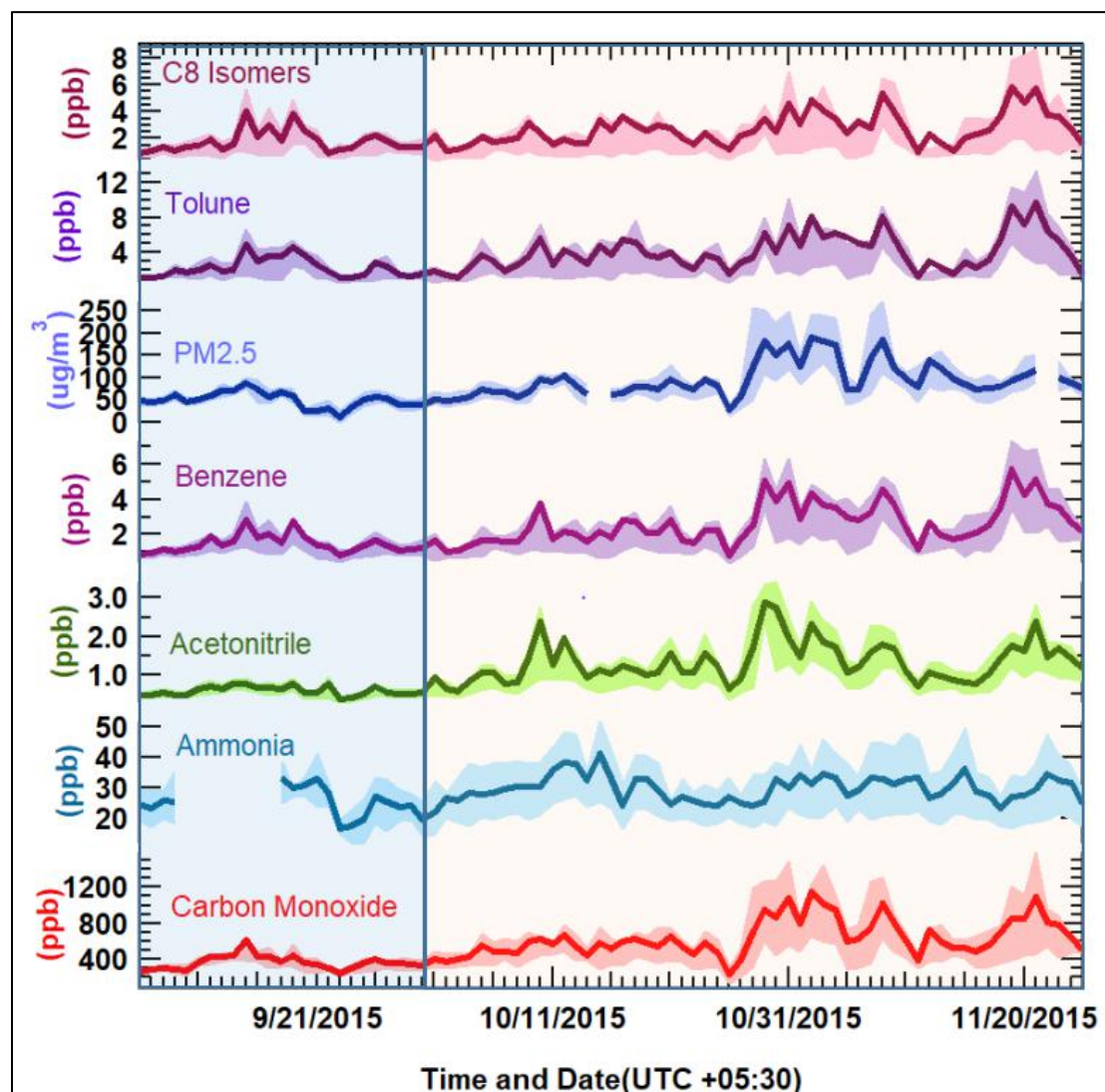


Figure 3.2.1: Time series of the daily averaged mixing ratios of (in the order, from bottom to top) carbon monoxide, ammonia, acetonitrile, benzene, PM2.5, toluene and C8 Aromatics (sum of xylenes and ethyl benzene) for September-November 2015. The top and bottom shaded region represents 75<sup>th</sup> and 25<sup>th</sup> percentile respectively. The area shaded in blue of every plot represents the pre harvest period time (September 6, 2015- October 4, 2015) whereas the region represented in orange shows the post harvest period (October 5, 2015 - November 25, 2015).

The average 4 min mixing ratios during September- November 2015 varied from; 135 ppb to 1585 ppb for CO, 11.8 ppb to 51.8 ppb for ammonia, 0.3 ppb to 3.4 ppb for acetonitrile, 0.4 ppb to 7.2 ppb for benzene, <1  $\mu\text{g}/\text{m}^3$  to 269  $\mu\text{g}/\text{m}^3$  for PM<sub>2.5</sub>, 0.5 ppb to 13.3 ppb for toluene and 0.3 to 8.7 ppb for C8 aromatics. It is quite clear from the time series, that enhancements in the mixing ratios were observed in the post harvest period with respect to pre harvest period for chemical species of carbon monoxide, benzene and benzenoids. Acetonitrile, a chemical signature for biomass burning, specifically showed intensified mixing ratio in the post harvest season on several days coupled with remotely sensed fire counts, makes a strong case for enhancement due to biomass burning activities.

<b>Gas Species</b>	<b>Pre Harvest Average(S.D.)</b>	<b>Post Harvest Average(S.D.)</b>
Ammonia (ppb)	25.4(4.6)	30.3(4.1)
PM2.5 ( $\mu\text{g}/\text{m}^3$ )	49.8(16.3)	99.0(38.9)
Acetonitrile (ppb)	0.6(0.1)	1.4(0.5)
Benzene (ppb)	1.4(0.5)	2.7(1.1)
Toluene (ppb)	2.2(1.0)	4.3(2.0)
C8 Aromatics (ppb)	1.7(0.8)	2.8(1.2)
CO (ppb)	369.2(74.5)	685.4(197.9)

Table 3.2.1 shows the gas species along with their mixing ratios in pre harvest and post harvest, the value in the bracket represents standard deviation.

The post harvest period (October 05- November 26) has ammonia daily averaged mixing ratio values greater than 27.7 ppb and peaks observed in daily average mixing ratio were observed on, November 13<sup>th</sup>,2015 with 34 ppb, November 16<sup>th</sup>,2015 with 38 ppb, November 17<sup>th</sup>,2015 with 41 ppb. It has been reported in previous studies that crop residue burning in the October-November over India emit CO,CH<sub>4</sub>, NO<sub>x</sub> and CO<sub>2</sub> (Gupta et al 2004) and similar behaviour is also observed for ammonia. From table 3.2.1 it was observed that the daily average mixing ratio enhancement for PM<sub>2.5</sub>, CO, acetonitrile, benzene, toluene, C8 aromatics and ammonia were by a factor of 1.9, 1.8, 2.3, 1.9, 1.9, 1.6 and 1.2 respectively. The 24 hour averaged PM<sub>2.5</sub> permissible

limit for industrial, residential and other areas is  $60 \mu\text{g}/\text{m}^3$  as per NAAQS,2009. In pre harvest season, this limit was exceeded 28 percent of the times whereas in the post harvest season, this limit exceeded 84 percent of the times clearly indicating the impact of paddy residue burning on the deterioration of air quality and ecosystem.

The gap in data for ammonia (09 to 17 September,2015) and  $\text{PM}_{2.5}$  (15 October and 22 November,2015) is due to the instrument down times pertaining to instrument maintenance.

The mixing ratios of CO (a marker of incomplete combustion), benzene and benzenoids and  $\text{PM}_{2.5}$  correlates with the mixing ratio of acetonitrile hinting at co-emission from biomass burning (Warneke et al. 2011). Table 3.2.2 is a correlation matrix for the post harvest season of all the species.

R value	PM2.5	CO	Acetonitrile	Benzene	Toluene	C8 Aromatics	Ammonia
PM2.5	<b>1.0</b>	<b>0.9</b>	<b>0.7</b>	<b>0.7</b>	<b>0.6</b>	<b>0.5</b>	0.2
CO	<b>0.9</b>	<b>1.0</b>	<b>0.8</b>	<b>0.9</b>	<b>0.8</b>	<b>0.8</b>	0.1
Acetonitrile	<b>0.7</b>	<b>0.8</b>	<b>1.0</b>	<b>0.8</b>	<b>0.7</b>	<b>0.6</b>	0.0
Benzene	<b>0.7</b>	<b>0.9</b>	<b>0.8</b>	<b>1.0</b>	<b>0.9</b>	<b>0.9</b>	0.0
Toluene	<b>0.6</b>	<b>0.8</b>	<b>0.7</b>	<b>0.9</b>	<b>1.0</b>	<b>0.9</b>	0.1
C8 Aromatics	<b>0.5</b>	<b>0.8</b>	<b>0.6</b>	<b>0.9</b>	<b>0.9</b>	<b>1.0</b>	0.0
Ammonia	0.2	0.1	0.0	0.0	0.1	0.0	<b>1.0</b>

Table 3.2.2 is a correlation matrix for the post harvest season of all the gas species done using daily averaged mixing ratios. Strong correlation(>0.5) is shown in bold.

Ammonia doesn't correlate with tracers emitted from biomass burning as it gets masked due to gas to particle phase conversion (further discussed in section 3.4).

### 3.3 Diel and box whisker plot of the primary data set

The paddy residue is usually burned in the late afternoon/evening hours under calm meteorological conditions to deceive state and local authorities (Kumar et al. 2015).

Figure 3.3.1 the average hourly diel profile of a) ammonia, b) acetonitrile, c) PM<sub>2.5</sub>, d) benzene, e)toluene, f) C8 aromatics(sum of xylenes and ethyl benzene), g) carbon monoxide quality controlled for the September- November,2015 period.

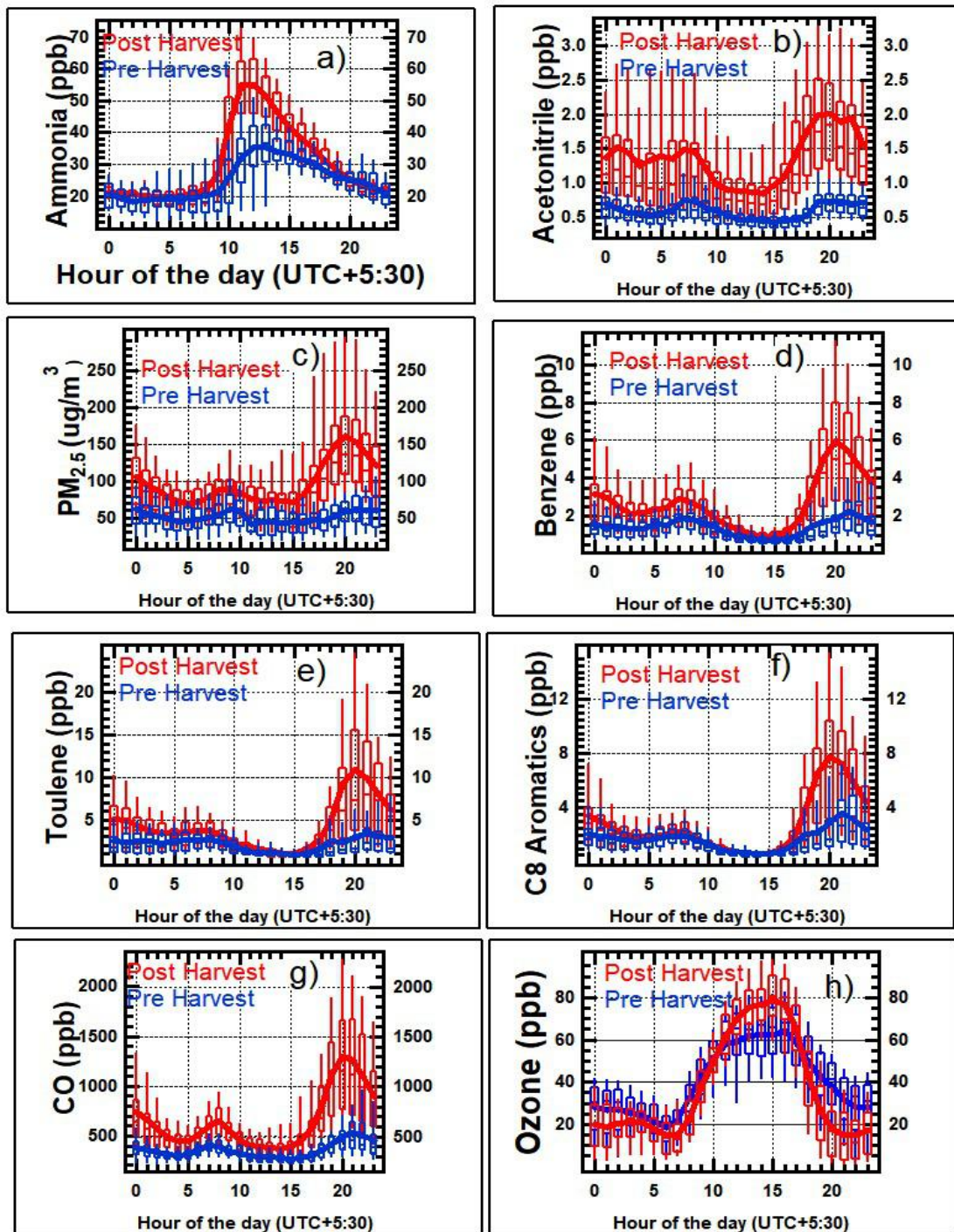


Figure 3.3.1 Diel box and whisker profiles of a) ammonia, b) acetonitrile, c) PM<sub>2.5</sub>, d) benzene, e)toluene, f) C8 aromatics(sum of xylenes and ethyl benzene), g) carbon monoxide h) ozone optimized for September- November,2015 period. The number of

data points for pre paddy harvest(n=10,438) and for post paddy harvest period(n=18,719), are denoted in the brackets, 4m averaged.

The pre paddy harvest diel box and whisker profile is shown in blue color and the post paddy harvest diel box and whisker profile is shown in red color. The hour of the day is represented on X axis and mixing ratios of the trace gases are represented on Y axis. The box is made up of three horizontal lines representing the 25<sup>th</sup>, 50<sup>th</sup> and 75<sup>th</sup> percentile, the line connects the hourly average and the whiskers represent the 10<sup>th</sup> and the 90<sup>th</sup> percentile of; the pre paddy harvest(n=10,438) and post paddy harvest period(n=18,719) dataset for each species, where n is the number of measurements.

The aromatic volatile organic compounds (VOCs) showed a bimodal profile with maxima at morning and evening and minima at late noon. Ammonia showcases an unimodal behaviour with maxima at noon and minima at night. The peak observed in the hourly averaged mixing ratio of ammonia starts at 09:00 and declines at 12:00 hour of the day. The decline in hourly averaged mixing ratio starts at 12:00 and occurs till 20:00 hour of the day. The hourly averaged mixing ratio remains almost constant from 20:00 to 09:00 hour of the day. Photochemically formed ozone, where the peak in hourly averaged mixing ratio starts from 10:00 to 15:00 hour of the day correlates with higher solar radiation, comparing it with ammonia: ammonia starts to decline at 12:00 hour at the day when the solar radiation is at the highest. The contribution therefore of photochemically formed species on ambient mixing ratio average is less.

An enhancement is clearly observed in the average hourly mixing ratios in post harvest season with respect to the pre harvest season of a) ammonia, b) acetonitrile, c) PM<sub>2.5</sub>, d) benzene, e) toluene, f) C8 aromatics (sum of xylenes and ethyl benzene), g) carbon monoxide and is observed at 16:00 to 20:00 hour of the day except for ammonia(09:00 to 12:00 h). The enhancement seen is, by the factor of 1.6 during 09:00 to 12:00 hour of the day and the enhancement for PM<sub>2.5</sub>, CO, acetonitrile, benzene, toluene, C8 aromatics were by a factor of 2.5, 2.2, 2.8, 2.6, 2.8 and 2.3 respectively during 16:00 to 20:00 hour of the day. During 16:00 to 20:00 hour of the day, events of biomass burning along with shallow boundary layer (50-100m) results in enhanced mixing ratio. In the case of acetonitrile the enhancement seen

from 16:00 to 20:00 (1.67 ppb in post harvest vs 0.6 ppb in the pre harvest) is significant.

During 10:00 to 15:00 hour of the day; VOCs like benzene, toluene and C8 aromatics have significantly shorter lifetime (faster reaction with OH radicals) than acetonitrile and carbon monoxide and therefore the intensification in the post harvest season is observed for these species is not significant.

The increase in the mixing ratios of chemical species from 15:00 is consistent with the information from rural local population on biomass burning activities (Chandra et al. 2016). From 12:00 to 15:00 hour of the day the height of the boundary layer(1500-2000m) is increasing and at maximum, therefore the air is well mixed and measured concentrations of chemical species is lessened, and the average diel concentration minima is observed. After sunrise and the breaking of the inversion layer, the reduction in the measured concentration. Similar enhancements are seen in PM<sub>2.5</sub>, benzene, toluene, sum of C8 aromatics and CO. Carbon monoxide shows a morning peak as well which represents burning of wood in the morning hours for household purposes, mainly heating of the water and cooking(further discussed in Sinha et al. 2014).

### **3.4 Chemical transformation of ammonia**

The peak, in the average hourly mixing ratio of ammonia during 09:00 to 12:00 is seen in both pre and (intensified in) post harvest season. This is due to the conversion of ammonium aerosol particles (as PM<sub>2.5</sub>) into ammonia gas, enabled by high ambient temperature and low relative humidity. The pollution peak (during 16:00 to 20:00 hour of the day) is not observed in ammonia because of the unfavourable conditions for aerosol to gas phase ammonia conversion; low ambient temperature and high relative humidity. PM<sub>2.5</sub> mass loading is increased in the post paddy harvest season, the enhanced concentration of PM<sub>2.5</sub> also results in enhanced gas phase ammonia during volatilization at 09:00 to 12:00 hour of the day. Post harvest burning enhances PM<sub>2.5</sub> concentration (co emitted with acetonitrile) which in turn increases

the ammonia concentration (solid to gas phase conversion of the ammonium aerosol), the pollution plume of ammonia gets masked in the post harvest season.

### 3.4.1 Anti Correlation with PM<sub>2.5</sub>

During the post harvest season, the peak observed at 09:00-12:00 hour of the day in ammonia concentration correlates with decrease in concentration of PM<sub>2.5</sub>, meaning the chemical transformation of solid phase ammonium particles into gas phase ammonia due to favourable conditions for the gas phase formation(3.4.2 discusses ammonia's relation with RH and ambient temp) with the  $r^2$  value of 0.94 representing strong correlation(figure 3.4.1.1,left). For ammonia, the absence of pollution peak(16:00 to 20:00 h) is due to the unfavourable conditions for gas phase ammonia to exist as gas phase (converted to solid phase ammonium aerosol particles) ammonia(figure 3.4.1.1,right) with the  $r^2$  value of 0.98 representing strong correlation.

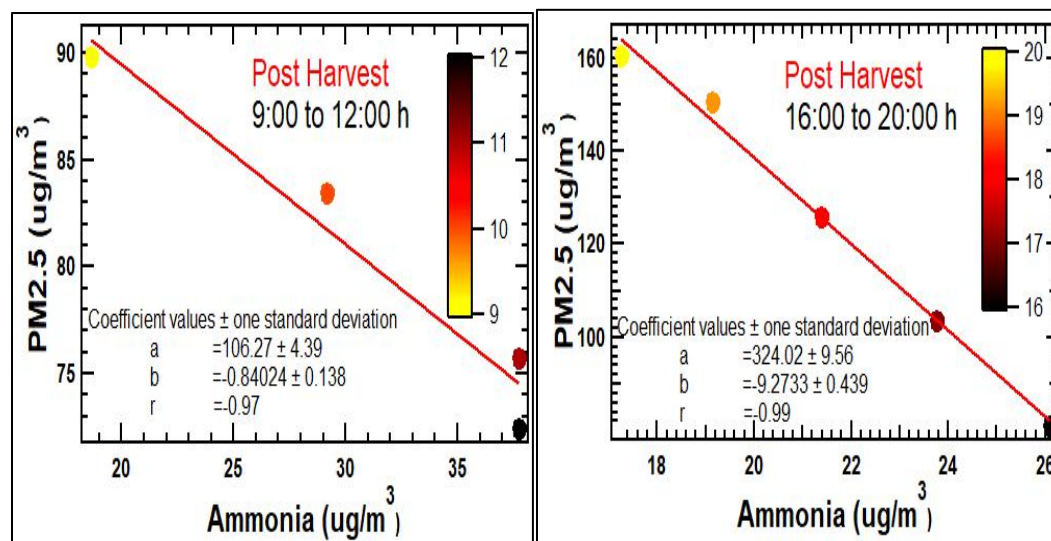


Figure 3.4.1.1(left) represents the correlation plot of hourly averaged ammonia and PM<sub>2.5</sub> during 09:00 to 12:00 h of the day with color scale yellow(09:00) to red(12:00), whereas(right) represents the correlation plot of hourly averaged ammonia and PM<sub>2.5</sub> during 16:00 to 20:00 h of the day with color scale yellow(20:00) to red(16:00), during the post harvest season.

During the pre harvest season, a similar peak is observed in the ammonia mixing ratio. This increase in concentration is also attributed to the favourable gas phase formation chemistry of inorganic PM<sub>2.5</sub> particles. Figure 3.4.1.2(left) represents the hourly averaged, ammonia concentration plotted with PM<sub>2.5</sub> concentration for the 09:00 to



12:00 hour of the day, representing an anti correlation between them with  $r^2$  value of 0.84 showing strong correlation, whereas figure 3.4.1.2(right) represents the hourly averaged concentration of ammonia and PM2.5 during 16:00 to 20:00h of the day showing anti correlation between the two with  $r^2$  value of 0.75.

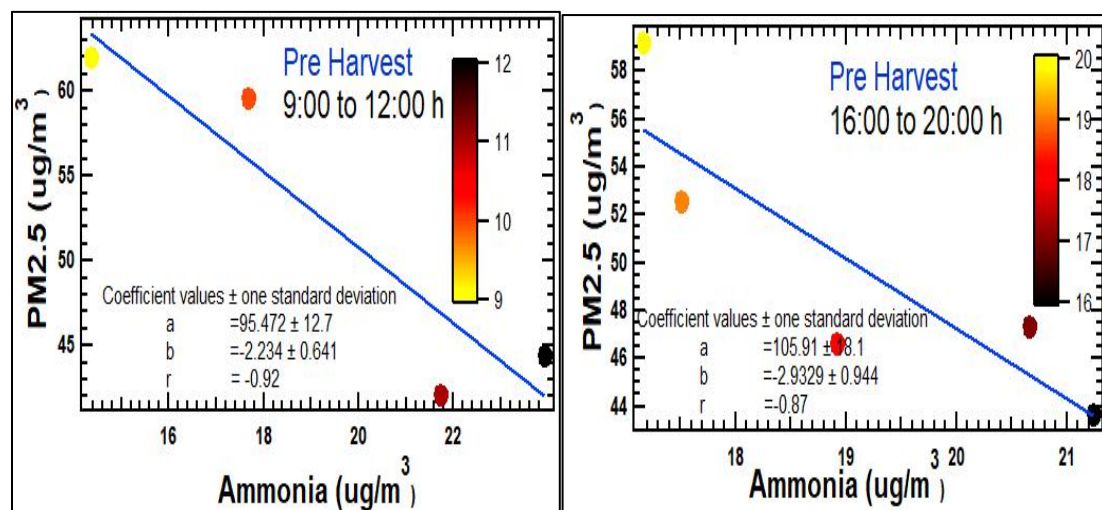


Figure 3.4.1.2 (left) represents the correlation plot of hourly averaged ammonia and PM2.5 during 09:00 to 12:00 h of the day with color scale yellow (09:00) to red (12:00), whereas (right) represents the correlation plot of hourly averaged concentration of ammonia and PM2.5 during 16:00 to 20:00 h of the day with color scale yellow (20:00) to red (16:00), during the pre harvest season.

### 3.4.2 Ammonia's relation with RH and ambient temperature

Ammonia's partition phase chemistry is vitally dependent upon relative humidity and ambient temperature. Figure 3.4.2.1 represents a plot between hourly averaged concentration of ammonia and ambient temperature, in the post harvest season. It is evident that at conditions of low temperature and high relative humidity (RH), the ammonia gas phase concentration found is low (found at bottom left of plot) usually at midnight. Whereas, at high temperature and low RH means existence of excessive gas phase ammonia found at the top right of the plot, which is observed at 09:00-14:00h of the day. The same trend is also found for the pre harvest period (figure 3.4.2.2).

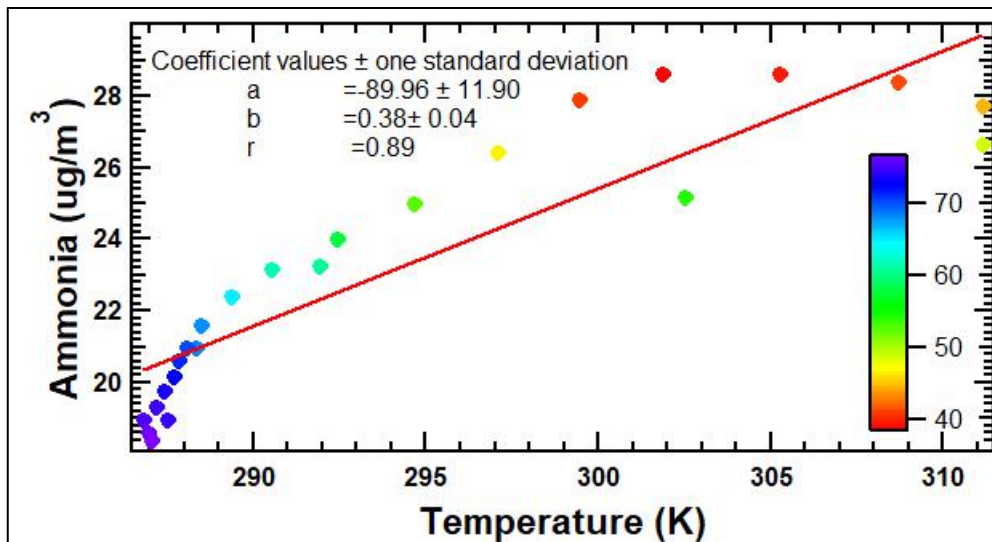


Figure 3.4.2.1 represents a plot between hourly averaged concentration of ammonia and ambient temperature, with  $r^2$  value of 0.79 in the post harvest season. The color scale represents the relative humidity.

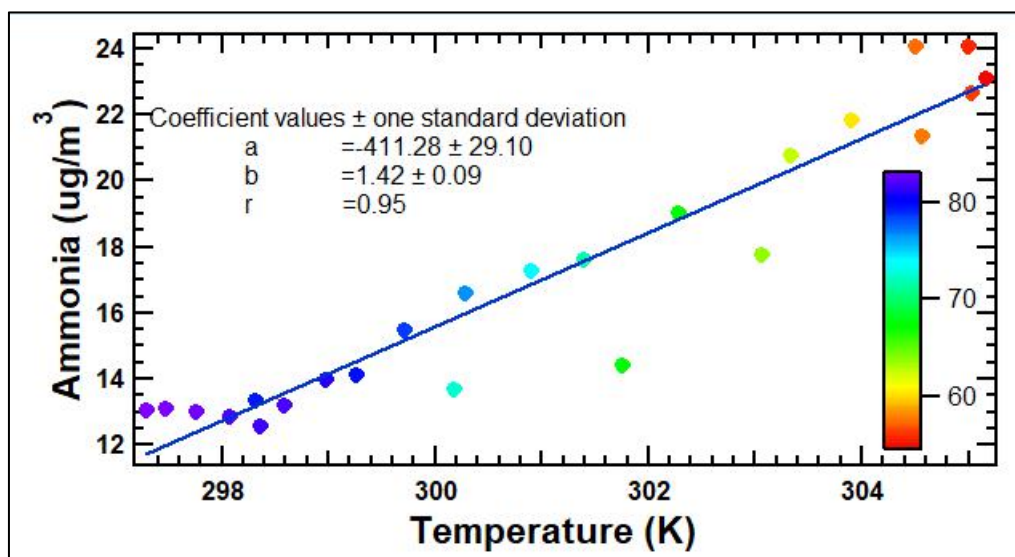


Figure 3.4.2.1 represents a plot between hourly averaged concentration of ammonia and ambient temperature, with  $r^2$  value of 0.90 in the pre harvest season. The color scale represents the relative humidity.

### 3.4.3 Temperature dependence of ammonium salts

Ammonium nitrate and ammonium chloride salts are temperature and pressure sensitive. The decomposition and formation reaction of these salts is reported in table 1.2.1. The equilibrium constant for R3 and R4 has been calculated with temperature dependence (Koziel et al. 2006). From figure 3.4.3.1, it is observed that the equilibrium constants are, significantly higher at higher temperature(32°C) for both , ( $80 \times 10^{-3}$ ) ammonium nitrate (left) and ( $14 \times 10^{-3}$ ) ammonium chloride (right) implying existence of solid to gas phase partitioning for both of these salts. Sudden increase in equilibrium constants are observed when the ambient temperature crosses 302K,implying partial thermal decomposition of ammonium salts.

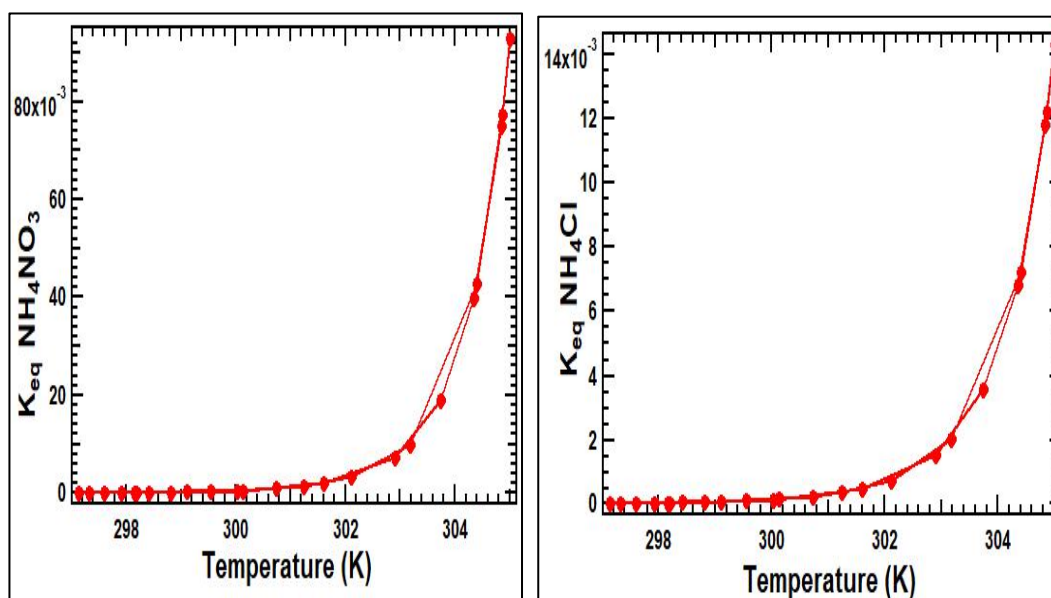


Figure 3.4.3.1 plot between equilibrium constant and temperature(K) for ammonium nitrate (left) and ammonium chloride (right), increase in temperature results in a higher equilibrium constants above 302K temperature.

The thermal stability of  $NH_4Cl$  is around 540K and  $NH_4NO_3$  is around 570K (Olszak-Humienik et al 2001). For reaction R3 with higher equilibrium constant for ammonium nitrate, the formation of gas phase ammonia would be more as compared to ammonium chloride (refer table 1.2.1 for R3 and R4 reactions). From figure 3.4.3.2 in the post harvest season, it can be observed that above 302K sudden increase in concentration of ammonium salts occur. The temperature dependent regime has more nitrate salts than chloride salts.

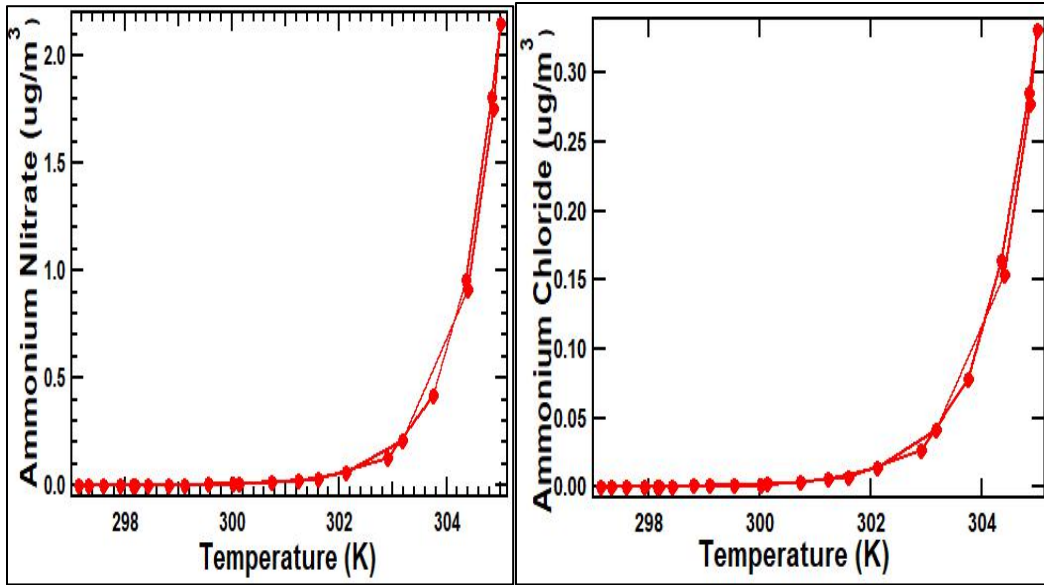


Figure 3.4.3.2 Hourly averaged ammonium nitrate (left) and ammonium chloride (right) concentration ( $\mu\text{g}/\text{m}^3$ ) dependence with temperature is plotted.

The equilibrium constant for ammonium nitrate is almost 5 times higher than that of ammonium chloride ( $80 \times 10^{-3}$  vs  $14 \times 10^{-3}$ ). At lower temperature, lower concentration of gas phase ammonia is observed with significantly lower equilibrium constants (in the range of  $10^{-7}$ ). However from figure 3.4.3.2 it is concluded that greater salt volatilisation to gas phase ammonia happens at temperature above 302K.

Figure 3.4.3.3 represents ammonia and ammonium nitrate and ammonium chloride's temperature relation at temperature higher than 302K.

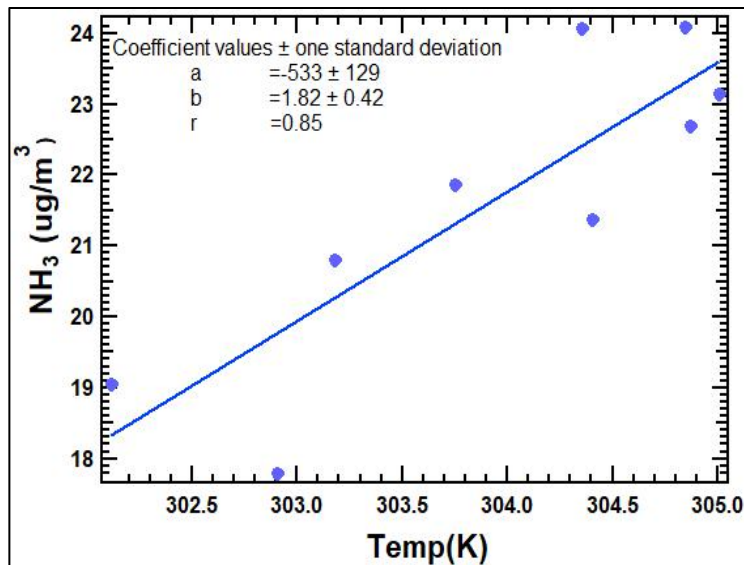


Figure 3.4.3.3 represents hourly averaged gas phase ammonia concentration's linear relation with temperature with  $r^2$  value of 0.72.

This gas phase ammonia is due to solid to gas phase conversion of ammonium salts. The temperature dependent equilibrium constants, help in approximating the gas phase ammonia concentration emitted from ammonium nitrate and ammonium chloride, and were used in calculating ammonium salts' temperature dependence at higher temperature. Figure 3.4.3.4 represents the hourly averaged concentration of ammonium nitrate (left) and ammonium chloride (right) relation with temperature higher than 300K with slope of 0.72 and 0.11 respectively.

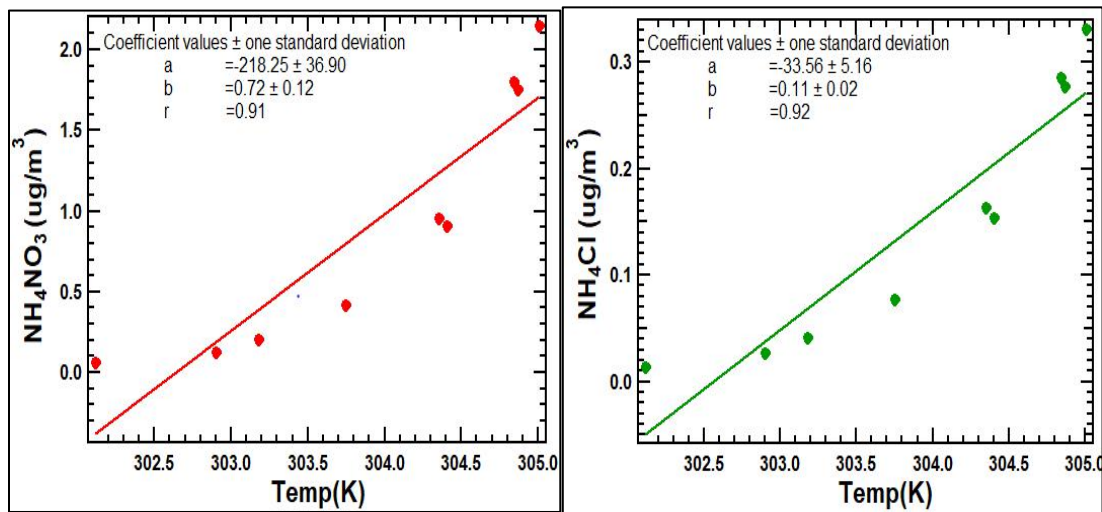


Figure 3.4.3.4 represents the hourly averaged concentration of ammonium nitrate (left) and ammonium chloride (right) relation with temperature higher than 300K with  $r^2$  value of 0.82 and 0.84 respectively

# Chapter 4

## Summary and conclusion

A new in-situ data set of ammonia, PM<sub>2.5</sub>, several VOCs and CO was quality controlled and analyzed for September to November, 2015 at a 4 minute temporal resolution using CRDS and other measurement techniques to study the effect of paddy residue burning on ammonia. A temporal variation of ammonia with other gases was investigated over the same time frame which led to the finding of enhancements in mixing ratio of all the observed chemical species in this study. The months of September to November were demarcated on the basis of remotely sensed fire activities and the enhancement observed in the acetonitrile data into pre harvest (06/09/2015 - 04/10/2015) and post harvest (05/10/2015- 26/11/2015). It was of priority to ascertain the consistency in the fetch region with meteorological evidences. The wind rose plot for the pre harvest and post harvest season showed consistency in fetch region as the wind direction remained pre dominantly north and northwest for almost 90 percent of the time and the wind speed remained in between 1-10 ms<sup>-1</sup> for about 85 percent of the time. The diel and box profile of ammonia showed the peak at 09:00-12:00 hour of the day in both pre and (intensified in) post harvest season and PM<sub>2.5</sub> showed a decline at same hours hinting at anti correlation between them. The correlation plot showed strong anti correlation between the two with r<sup>2</sup> values greater than 0.50, in both pre and post harvest season concluding aerosol to gas phase conversion of inorganic PM<sub>2.5</sub> particles to gas phase ammonia. It was further observed that during 16:00- 20:00 hour of the day, there was a peak in concentration of PM<sub>2.5</sub> but absent in ammonia. Gas phase ammonia was getting transformed into solid phase inorganic PM<sub>2.5</sub> particles with higher relative humidity and lower temperature providing favourable gas to solid phase conversion conditions. Gas phase ammonia concentration's relation with ambient temperature was studied and it was concluded that higher gas phase ammonia's presence is due to particle phase volatilization mainly of ammonium chloride and ammonium nitrate. At ambient temperature higher than 302K, linear strong correlation was seen of ammonium salts with ambient temperature. There is a need to better understand such multiphase

atmospheric chemistry of ammonia in the NW-IGP region which has adverse effects on humans and ecology.

# Bibliography

1. Allen, A.G., Harrison, R.M. and Erisman, J.-W. (1989). Field measurements of the dissociation of ammonium nitrate and ammonium chloride aerosols. *Atmospheric Environment* (1967), 23(7), pp.1591–1599.
2. Andreae, M.O. and Merlet, P. (2001). Emission of trace gases and aerosols from biomass burning. *Global Biogeochemical Cycles*, 15(4), pp.955–966.
3. Aneja, V. (2001). Atmospheric nitrogen compounds II: emissions, transport, transformation, deposition and assessment. *Atmospheric Environment*, 35(11), pp.1903–1911.
4. Aneja, V.P., Schlesinger, W.H., Erisman, J.W., Behera, S.N., Sharma, M. and Battye, W. (2012). Reactive nitrogen emissions from crop and livestock farming in India. *Atmospheric Environment*, 47, pp.92–103.
5. Ansari, A.S. and Pandis, S.N. (1998). Response of Inorganic PM to Precursor Concentrations. *Environmental Science & Technology*, 32(18), pp.2706–2714.
6. Ansari, A.S. and Pandis, S.N. (2000). The effect of metastable equilibrium states on the partitioning of nitrate between the gas and aerosol phases. *Atmospheric Environment*, 34(1), pp.157–168.
7. Asman, W. (2001). Modelling the atmospheric transport and deposition of ammonia and ammonium: an overview with special reference to Denmark. *Atmospheric Environment*, 35(11), pp.1969–1983.
8. Badarinath, K.V.S., Kumar Kharol, S. and Rani Sharma, A. (2009). Long-range transport of aerosols from agriculture crop residue burning in Indo-Gangetic Plains—A study using LIDAR, ground measurements and satellite data. *Journal of Atmospheric and Solar-Terrestrial Physics*, 71(1), pp.112–120.
9. Baek, B.H., Aneja, V.P. and Tong, Q. (2004). Chemical coupling between ammonia, acid gases, and fine particles. *Environmental Pollution*, 129(1), pp.89–98.
10. Behera, S.N. and Sharma, M. (2010). Investigating the potential role of ammonia in ion chemistry of fine particulate matter formation for an urban environment. *Science of The Total Environment*, 408(17), pp.3569–3575.
11. Behera, S.N. and Sharma, M. (2011). Degradation of SO<sub>2</sub>, NO<sub>2</sub> and NH<sub>3</sub> leading to formation of secondary inorganic aerosols: An environmental chamber study. *Atmospheric Environment*, 45(24), pp.4015–4024.



12. Behera, S.N., Sharma, M., Aneja, V.P. and Balasubramanian, R. (2013). Ammonia in the atmosphere: a review on emission sources, atmospheric chemistry and deposition on terrestrial bodies. *Environmental Science and Pollution Research*, [online] 20(11), pp.8092–8131. Available at: <https://meas.ncsu.edu/airquality/pubs/pdfs/149.pdf> [Accessed 12 Sep. 2019].
13. Chandra, B.P. and Sinha, V. (2016). Contribution of post-harvest agricultural paddy residue fires in the N.W. Indo-Gangetic Plain to ambient carcinogenic benzenoids, toxic isocyanic acid and carbon monoxide. *Environment International*, 88, pp.187–197.
14. Chandra, B.P., Sinha, V., Hakkim, H. and Sinha, B. (2017). Storage stability studies and field application of low cost glass flasks for analyses of thirteen ambient VOCs using proton transfer reaction mass spectrometry. *International Journal of Mass Spectrometry*, 419, pp.11–19.
15. Crosson, E.R. (2008). A cavity ring-down analyzer for measuring atmospheric levels of methane, carbon dioxide, and water vapor. *Applied Physics B*, 92(3), pp.403–408.
16. Du, Z., Mo, J. and Zhang, Y. (2014). Risk assessment of population inhalation exposure to volatile organic compounds and carbonyls in urban China. *Environment International*, 73, pp.33–45.
17. Huang, X., Song, Y., Li, M., Li, J., Huo, Q., Cai, X., Zhu, T., Hu, M. and Zhang, H. (2012). A high-resolution ammonia emission inventory in China. *Global Biogeochemical Cycles*, 26(1), p.n/a-n/a.
18. Leytem, A.B. and Rotz, C.A. (2016). 1289 Reactive nitrogen losses from dairy production systems. *Journal of Animal Science*, 94(suppl\_5), pp.622–622.
19. Reis, S., Pinder, R.W., Zhang, M., Lijie, G. and Sutton, M.A. (2009). Reactive nitrogen in atmospheric emission inventories. *Atmospheric Chemistry and Physics*, 9(19), pp.7657–7677.
20. Saraswati, George, M.P., Sharma, S.K., Mandal, T.K. and Kotnala, R.K. (2018). Simultaneous Measurements of Ambient NH<sub>3</sub> and Its Relationship with Other Trace Gases, PM<sub>2.5</sub> and Meteorological Parameters over Delhi, India. *MAPAN*, 34(1), pp.55–69.
21. Saraswati, Sharma, S.K. and Mandal, T.K. (2017). Five-year measurements of ambient ammonia and its relationships with other trace gases at an urban site of Delhi, India. *Meteorology and Atmospheric Physics*, 130(2), pp.241–257.
22. Schlesinger, W. and Hartley, A. (1992). A global budget for atmospheric NH<sub>3</sub>. *Biogeochemistry*, 15(3).

23. Schurath, U. (1997). Atmospheric aerosols - sources and sinks of reactive trace gases. *Journal of Aerosol Science*, 28, pp.S31–S33.
24. Sharma, M., Kishore, S., Tripathi, S.N. and Behera, S.N. (2007). Role of atmospheric ammonia in the formation of inorganic secondary particulate matter: A study at Kanpur, India. *Journal of Atmospheric Chemistry*, 58(1), pp.1–17.
25. Sinha, V., Kumar, V. and Sarkar, C. (2014). Chemical composition of pre-monsoon air in the Indo-Gangetic Plain measured using a new air quality facility and PTR-MS: high surface ozone and strong influence of biomass burning. *Atmospheric Chemistry and Physics*, 14(12), pp.5921–5941.
26. Stockwell, C.E., Veres, P.R., Williams, J. and Yokelson, R.J. (2015). Characterization of biomass burning emissions from cooking fires, peat, crop residue, and other fuels with high-resolution proton-transfer-reaction time-of-flight mass spectrometry. *Atmospheric Chemistry and Physics*, 15(2), pp.845–865.
27. Sutton, M. and Fowler, D. (2002). Introduction: fluxes and impacts of atmospheric ammonia on national, landscape and farm scales. *Environmental Pollution*, 119(1), pp.7–8.
28. Toxicological Review of Ammonia. (2016). EPA. Noncancer Inhalation: Executive Summary.
29. Venkataraman, C., Habib, G., Kadamba, D., Shrivastava, M., Leon, J.-F., Crouzille, B., Boucher, O. and Streets, D.G. (2006). Emissions from open biomass burning in India: Integrating the inventory approach with high-resolution Moderate Resolution Imaging Spectroradiometer (MODIS) active-fire and land cover data. *Global Biogeochemical Cycles*, 20(2), p.n/a-n/a.
30. Wang, S., Nan, J., Shi, C., Fu, Q., Gao, S., Wang, D., Cui, H., Saiz-Lopez, A. and Zhou, B. (2015). Atmospheric ammonia and its impacts on regional air quality over the megacity of Shanghai, China. *Scientific Reports*, 5(1).
31. Warneke, C., Roberts, J.M., Veres, P., Gilman, J., Kuster, W.C., Burling, I., Yokelson, R. and de Gouw, J.A. (2011). VOC identification and inter-comparison from laboratory biomass burning using PTR-MS and PIT-MS. *International Journal of Mass Spectrometry*, 303(1), pp.6–14.